Probing the Effects of Pathogenic Mutations on Prion-like Conversion of Superoxide dismutase-1

by

Bahareh Hamzeh

A thesis submitted in partial fulfillment of the requirements for the degree of

Master of Science

Department of Physics
University of Alberta

Abstract

Multiple neurodegenerative diseases feature the accumulation of misfolded proteins in and around neurons. In some cases, misfolding propagates through a prion-like mechanism whereby interactions between misfolded conformers and natively folded conformers induce the latter to convert into the misfolded conformer. We developed a novel assay to monitor the prion-like conversion of superoxide dismutase-1 (SOD1), whose misfolding is linked to amyotrophic lateral sclerosis (ALS). In this assay, a misfolded SOD1 mutant monomer that is associated with familial ALS is tethered to a wild-type (wt) SOD1 monomer, and the enzymatic activity of the wt SOD1 domain is monitored over time to detect its conversion into inactive misfolded conformers. Tethering the mutant vastly increases the effective local concentration of misfolded protein in the assay while keeping the global concentration low, decoupling conversion from aggregation. Our study tested this assay on a range of SOD1 heterodimers, including wt-G85R, wt-G127X, wt-D76V, wt-G93A, wt-G41D, wt-I104F, wt-G41S, and wt-A4V.

The results varied significantly among different mutants. We observed distinct patterns in the enzymatic activity of these heterodimers, with some exhibiting a sigmoidal decline, suggestive of a direct conversion process. This decline was characterized by a stable phase of activity, followed by a decrease representing the conversion phase, and finally reaching stability again, suggesting the completion of the conversion. In contrast, other heterodimers demonstrated a pattern of stability with no obvious change in activity, suggesting either a slower conversion rate or retention of some activity in the mutant domain. One specific heterodimer, wt-I104F, showed a more complex or biphasic decline in its activity, suggesting the heterodimer may undergo two separate processes.

Our findings challenge our initial assumptions about the relationship between the rapidity of ALS progression and the conversion rate of wt SOD1. The lack of a direct correlation between these factors suggests a more intricate mechanism underpinning ALS progression than previously understood. This research lays the groundwork for future studies to develop a more nuanced understanding of the prion-like conversion process in ALS. Future directions include refining our assay technique to explore a broader range of SOD1 mutants and investigating the potential therapeutic applications of targeting specific stages or mechanisms of the SOD1 conversion process. By deepening our understanding of SOD1 misfolding and its prion-like propagation in ALS, we aim to open new avenues for developing effective treatments for this disabling disease.

Preface

The research in this thesis is the original work of Bahareh Hamzeh, carried out under the supervision of Dr. Michael T. Woodside in the Department of Physics at the University of Alberta. The study focused on SOD1 heterodimers, which were designed by Dr. Abhishek Narayan and Dr. Michael T. Woodside. Bahareh Hamzeh was responsible for producing and purifying the heterodimers wt-G85R, wt-G127X, wt-A4V, wt-I104F, wt-G41D, wt-G41S, wt-D76V, and wt-G93A. Dr. Abhishek Narayan did the production and purification of the SOD1 homodimer wt-wt. Dr. Abhishek Narayan also measured the activity of wt-wt, wt-G85R, and wt-G127X, while Bahareh Hamzeh measured the activity of all the other SOD1 heterodimers.

This thesis also benefited from the help of ChatGPT, a language tool from OpenAI. ChatGPT helped improve the English in the thesis, fixing grammar and spelling mistakes and selecting more appropriate vocabulary. However, the final content, including the word choices and main ideas, was decided and confirmed by Bahareh Hamzeh.

This thesis is respectfully dedicated to my uncle, Roli, who bravely battled ALS and passed away at a young age. His courage and struggle have been a profound inspiration for this research, motivating me to contribute, even in a small way, towards finding a cure for ALS.

Acknowledgement

Firstly, I would like to express my deepest gratitude to my supervisor, Dr. Michael T. Woodside, who guided me through this research path with his insightful feedback, generous support, patience, and kindness. Working as a member of his research team taught me the importance of academic research in terms of collaboration, responsibility, precision, repetition and stamina. I am also grateful for the opportunity to conduct my research in the department's well-furnished laboratories.

I am deeply thankful to Craig Garen for his invaluable assistance and patience in teaching me numerous lab techniques, which played a significant role in my research endeavors. His guidance has been indispensable throughout this journey.

I would like to extend my appreciation to Dr. Abhishek Narayan for his invaluable assistance. His explanations of various lab techniques and his generous provision of essential information were instrumental in completing my thesis.

Special thanks are due to my thesis committee members, Dr. Michael T. Woodside, Dr. Daniel Charlebois, and Dr. Lindsay LeBlanc, for their constructive criticism and encouragement, which greatly enhanced the quality of my thesis.

I express my gratitude to every member of the Woodside Lab for their constant support and for patiently addressing my questions and uncertainties. I would especially like to thank my office mate and research fellow, Rohith, whose willingness to help with a range of issues, both big and small, has not only aided my research but also made my experience much more enjoyable and fulfilling.

Special mention goes to my friends at the U of A – Hamid, Niloufar, Nakul, and Samira – for their companionship, empathy, and unwavering moral support through life's highs and lows. Their presence has greatly enriched my life, giving me a sense of family here.

I am deeply grateful to my parents and my partner, Farzan, for their constant support and encouragement and their unshakable faith in me. Their support has been a crucial factor in making this journey less daunting.

Contents

List of Tables

List of Figures

List of Symbols, Nomenclatures and Abbreviations

6XSB	6X Sample Buffer
Aβ	Amyloid-beta
AA	Amino Acid
AD	Alzheimer's Disease
ALS	Amyotrophic Lateral Sclerosis
APS	Ammonium Persulphate
BCS	Bathocuproinedisulfonic Acid
BL21	A strain of the bacterium E. coli
BL21 (DL3)	A variant or a specific designation of the BL21 strain of E. coli
BSA	Bovine Serum Albumin
BSE	Bovine Spongiform Encephalopathy
DETAPAC	Diethylenetriaminepentaacetic Acid
DNase I	Deoxyribonuclease I
E. coli	Escherichia Coli
ECSOD	Extracellular Superoxide Dismutase
EDTA	Ethylenediaminetetraacetic acid
fALS	Familial Amyotrophic Lateral Sclerosis
FECs	Force-Extension Curves
FRET	Förster Resonance Energy Transfer
FUS	Fused in Sarcoma
GPx	Glutathione Peroxidase
HEWL	Hen Egg White Lysozyme
IPTG	Isopropyl-β-D-thiogalactopyranoside
LB	Lysogeny Broth
MWCO	Molecular Weight Cut-off
MWT	Molecular Weight Ladder
NDDs	Neurodegenerative Diseases
Ni^{2+}-IMAC	Nickel Ion Immobilized Metal Affinity Chromatography
OD	Optical Density
OD595	Optical Density at 595 nm
PB	Potassium Phosphate Buffer
PD	Parkinson's Disease
PrP	Prion Protein
ROS	Reactive Oxygen Species
rpm	Revolutions Per Minute
sALS	Sporadic Amyotrophic Lateral Sclerosis
SDS-PAGE	Sodium Dodecyl Sulphate–Polyacrylamide Gel Electrophoresis

SEM	Standard error of the mean
SMFS	Single-Molecule Force Spectroscopy
SOD	Superoxide Dismutase
TARDBP	TAR DNA-Binding Protein
TCEP	Tris (2-carboxyethyl) phosphine
TEMED	N, N, N', N'-Tetramethylethylenediamine
Tris	Tris(hydroxymethyl)aminomethane
WST-1	Water-Soluble Tetrazolium
wt	Wild Type
XO	Xanthine Oxidase

Chapter 1: Introduction

1.1 Neurodegenerative Diseases and Propagated Misfolding

Numerous proteins can misfold, forming non-native structures that may lead to various diseases. Several neurodegenerative diseases (NDDs) are closely associated with protein misfolding [1]. Diseases like kuru and Creutzfeldt-Jakob disease in humans, scrapie in sheep, bovine spongiform encephalopathy (BSE, commonly known as "mad cow" disease), and chronic wasting disease in deer and elk are all linked to the misfolding of the prion protein (PrP) [2]. In Alzheimer's disease (AD), the misfolding of amyloid-beta (Aβ) and tau proteins is a key pathological feature [3], [4]. Parkinson's disease (PD) is characterized by the misfolding of the alpha-synuclein protein [5]. Amyotrophic lateral sclerosis (ALS) involves the misfolding of superoxide dismutase-1 (SOD1) and some other proteins [6]. These diseases exhibit gradual and irreversible dysfunction of neurons and synapses within specific nervous system regions, leading to distinctive clinical symptoms and progression [7], [8]. Genetic, environmental, and age-related internal factors are recognized as significant contributors to neurodegeneration; however, their pathogenic role and molecular mechanisms remain elusive [9], [10].

Misfolding in protein structure can be propagated, a behavior that was seen for the first time in prion disease [11]. It is generally acknowledged that prion diseases have been associated with the misfolded form of the prion protein, known as the scrapie prion protein or PrP^{Sc} [12]. Unlike the replication seen in organisms such as viruses and bacteria in infectious diseases, prion diseases are propagated by the conversion of natively folded structures by misfolded ones, which makes this transmission method distinctive [13]. In prion diseases, the cellular PrP (PrP^{C}) transforms into a transmissible misfolded version of this protein (PrP^{Sc}). During this transformation, the entire helical structure of the protein is restructured into β-sheets [14], leading

to some physicochemical attribute changes in PrP [2]. Therefore, the stable misfolded protein has the ability to transform the native form of the prion protein, facilitating its own propagation [15], [16]. In addition to prion proteins, several other proteins linked to NDDs have shown prion-like properties. These proteins, when misfolded, can interact with natively folded proteins and induce the native form to adopt the misfolded structure. This phenomenon is particularly evident in Alzheimer's, Parkinson's, and ALS diseases, where the propagation of their specific linked misfolded proteins acts as a toxic factor [17], [18], [19].

Prion-like propagation makes a therapeutic target, although directly assessing the conversion has been challenging, which hinders the development of therapeutic interventions for several disease-related proteins. This research investigates the conversion of wild-type SOD1 by specific mutations of SOD1. To tackle these limitations, we developed an assay to track the prion-like conversion of this protein, given its association with ALS. This assay employs a novel strategy: tethering a misfolded SOD1 mutant monomer to a natively folded or wild-type (wt) SOD1 monomer. Monitoring the enzymatic activity of the wt SOD1 over time lets us identify its shift into non-active misfolded conformers. This tethering method amplifies the effective local concentration of the misfolded protein in the assay, accelerating conversion while avoiding the aggregation that would normally occur at high concentrations. Applying this assay, we tested several SOD1 mutants linked to familial ALS and associated with different patient survival times. Outcomes were mixed; while some mutants showed conversion over some amount of time, others did not show any decrease in their activity, suggesting the conversion in their structure may not be the main reason for their impact on ALS. This work emphasizes that conversion and aggregation are distinct processes and introduces a new assay useful for exploring mechanisms of prion-like conversion in ALS and testing therapeutics to prevent conversion.

1.2 Superoxide dismutase-1 (SOD1) as a Prion-like Protein

1.2.1 Amyotrophic Lateral Sclerosis (ALS)

ALS is a neurodegenerative disorder that degenerates nerve cells inside the brain and spinal cord, controlling muscles and resulting in gradually weakening muscles, typically causing death due to breathing complications 2-5 years after the first signs appear [20]. People with ALS may have difficulty chewing and swallowing food, speaking, breathing, maintaining weight and receiving adequate nutrients. Ultimately, these people will lose their ability to walk or stand, use their arms and hands or even breathe independently. Since their cognitive abilities remain the same, they are aware of their gradual loss of function, which can lead to anxiety and depression complications [21].

ALS is classified into two main categories based on its heritability. The first, known as sporadic ALS (sALS), occurs randomly in individuals without any prior family history, accounting for approximately 90% of all ALS cases. Familial ALS (fALS) represents the remaining 10 % of cases and is associated with a family history of the disease [22]. Age plays a vital role in ALS, as most ALS patients are between 50 and 75 years [23]. The population of people over 60 is expected to increase globally, especially in developing countries, where the population of older people will grow from 9% in 2015 to 16% in 2040 [24]. Based on this pattern, the number of people suffering from chronic diseases, including ALS, has risen [25]. About 1.9 people out of 100,000 are diagnosed with ALS per year [26]. Even though it is rare, the social and economic effects of this disease are significant. Projections estimate that by 2040, the number of ALS cases will increase by about 69%, and approximately 400,000 people will suffer from this fatal diagnosis due to the aging of the population [23]. The underlying causes and mechanisms of ALS, whether familial or sporadic, are unclear, limiting the number of effective disease-modifying treatments. The most

established and widely recognized approved medications for this disorder are Riluzole, which increases the survival time by 2 to 3 months and has minimal impact on the quality of life [27], and Edaravone, which helps with movement ability but does not arrest the progression of the disease [28]. The lack of effective treatments results in increased genetic and molecular investigations on ALS's mechanisms to have a better understanding of the disease's behavior at the cell level. Up to now, at least 40 genes have been known to be associated with ALS. 4 genes, *SOD1*, *TAR DNA-binding protein* (*TARDBP*), *fused in sarcoma* (*FUS*) and *chromosome 9 open reading frame 72* (*C9orf72*) have accounted for about 60% and 11% of fALS and sALS cases respectively (Figure 1), which means they play the most significant role between genes in ALS [6].

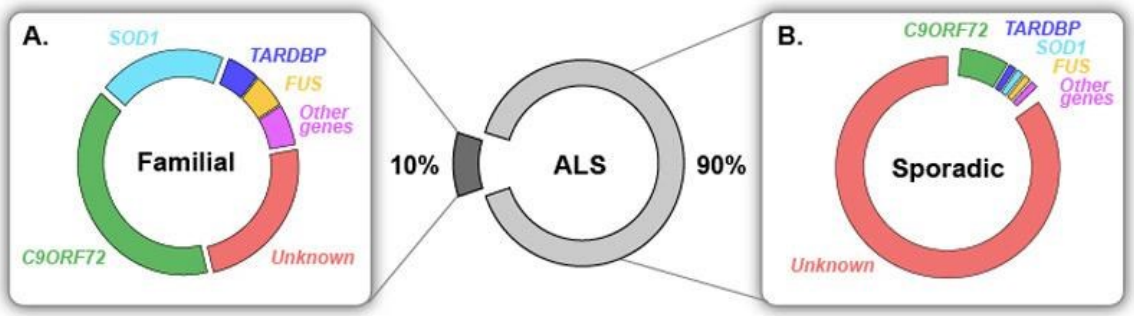

Figure 1. Most significant genes associated with familial ALS and sporadic ALS. This figure is adapted from [29].

1.2.2 Antioxidant Enzymes

In many aerobic metabolic cell processes, reactive oxygen species (ROS), such as hydrogen peroxide and superoxide, are generated. These species interact with DNA, lipids, and proteins. ROS can have different biological effects on intracellular targets based on their concentration. Although decreased levels of ROS are essential for controlling some critical physiological functions, high levels of them, which are present during oxidative stress, are cytotoxic and can lead to cellular damage and, on a larger scale, may lead to the onset of various diseases [30], [31]. The concentration of ROS within cells is determined by both its production and elimination provided by the antioxidant system. Three main antioxidant enzymes that exist in mammalian cells, essential for oxygen metabolizing cells, are glutathione peroxidase (GPx), catalase, and superoxide dismutase (SOD). SODs interact with superoxide radicals(O_2^-) and turn them into hydrogen peroxide(H_2O_2) and oxygen, while the Catalase and GPx interact with hydrogen peroxide and change it to water; catalase additionally converts it to water and oxygen. The total outcome is that potentially dangerous molecules are turned into water and oxygen [30]. SODs play the first and most crucial role in antioxidant enzyme systems against ROS.

Currently, three distinct versions of SOD have been recognized in mammals [31]. Two of these versions containing copper (Cu) and zinc (Zn) in their structure are CuZnSOD or SOD1, which exists in the cytoplasm, nucleus and Lysosomes of a cell [32] and extracellular SOD or ECSOD, which is located extracellularly in some tissues. The third version of SOD, known as MnSOD or SOD3, contains manganese in its structure and is positioned in the mitochondria of a cell [30]. Therefore, multiple forms of these enzymes alleviate oxidative stress in different parts of the cell. As a result, even if antioxidant proteins have similar enzymatic actions because they are located in different parts of a cell, they may have different effects after modulation.

1.2.3 Superoxide dismutase-1 (SOD1)

Prion diseases represent typical cases of NDDs, with a substantial body of evidence supporting the notion that prion-like conversion mechanisms entirely cause these diseases [33]. Unlike prion diseases, the cause of ALS is more complex. The biological function of PrP is not yet known exactly, which means that functional assays cannot be used to determine whether PrP has undergone prion-like conversion. Thus, more complicated structural assays are required, making the prion conversion study not very convenient. SOD1, on the other hand, is an enzyme protein whose prion-like conversion can be measured by simply determining whether it actively functions. Furthermore, PrP linked to prion diseases is a monomer but an oligomer, which makes it extremely challenging to replicate using recombinant protein approaches. Therefore, brain-purified material is required for reliable analysis. These limitations considerably contribute to the complexity and difficulty of studying prion conversion and experimental work with PrP. Considering these factors, SOD1 offers a more accessible model for investigating prion-like conversion processes.

SOD1 is not only the first gene that has been recognized in ALS pathogenesis, but it is also the most extensively studied among all the causative genes for the disease [34]. In the human body, SOD1, with a mass of 32,000 Da, is a dimer composed of two identical subunits. Each subunit comprises 153 amino acids, one copper and one zinc ion [35] (Figure 2).

Currently, more than 220 mutations of SOD1 have been linked to familial ALS [36]. These mutations are mainly associated with a gain of toxic function due to the misfolding of the SOD1 protein rather than solely a loss of its normal antioxidative function. While the loss of function may contribute to some extent, the gain of toxic function of misfolded SOD1 protein is believed to play a central role in the pathogenesis of the disease [37]. The precise role of all SOD1 mutations

associated with ALS is still unclear whether they cause, contribute to, modify the disease, or coexist with it. In our study, we delve into some such mutations to better understand their potential contributions to the progression of ALS. In this research, we investigate the prion-like conversion of wt SOD1 by eight SOD1 mutants, wt-G85R, wt-G127X, wt-D76V, wt-G93A, wt-G41D, wt-I104F, wt-G41S, and wt-A4V.

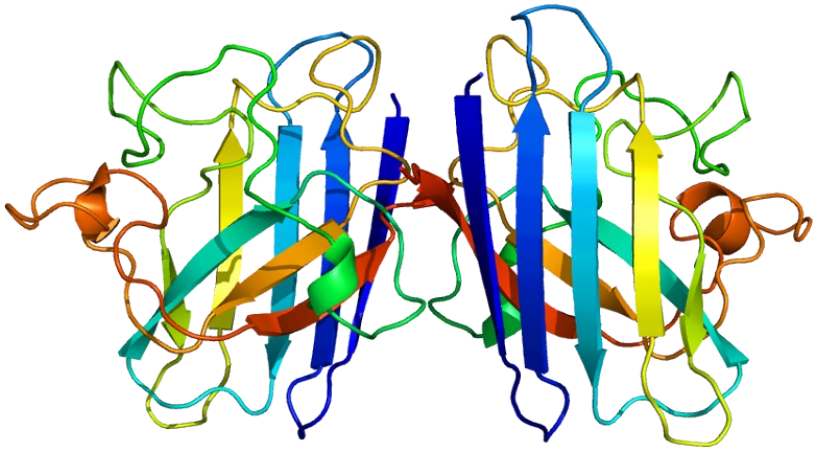

Figure 2. The structure of SOD1 protein in the human body. This figure is adapted from [38].

1.3 Protein Structure, Folding and Misfolding

Genetic data is preserved and transmitted through a one-dimensional sequence of DNA base pairs. For this information to be translated into biological function, the DNA sequence is transcribed to form messenger RNA (mRNA), which happens in the nucleus of a cell; the ribosome reads the mRNA sequence and translates it into a chain of amino acids (AAs) configuring protein [39] (Figure 3).

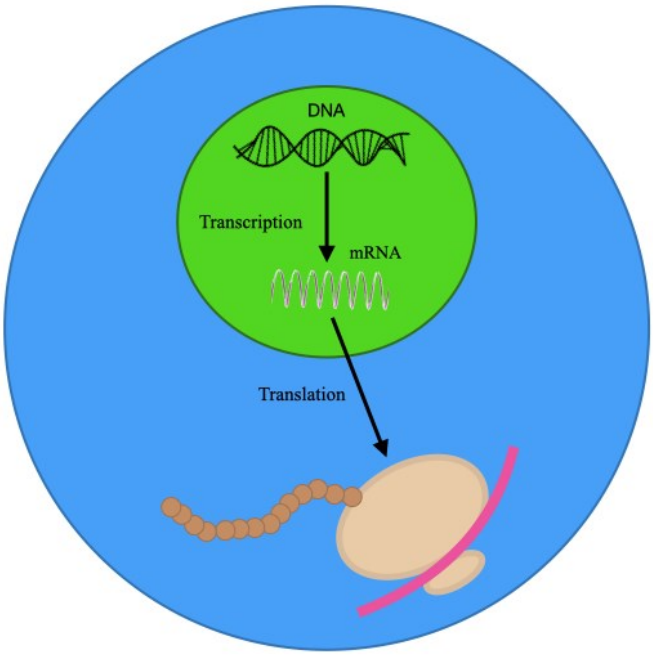

Figure 3. A simplified model of protein synthesis. Inside the cell nucleus, an mRNA molecule is generated during the transcription process. The transcript is then translated into a protein with the assistance of the ribosome molecules. Finally, protein folds in its 3D structure.

To play its role in the cell, a protein must fold into its native three-dimensional shape; therefore, the three-dimensional configuration of protein is crucial as it essentially dictates the protein's functionality [40]. The energy landscape concept can help us understand the complex protein folding and misfolding process. An energy landscape represents the energy for every imaginable form a protein might adopt. In theory, there are countless conformations a protein could take on this landscape; however, it settles into its tertiary structure. This tertiary form emerges from the protein's secondary structure, which is composed of helices, strands/sheets, and loops formed through interactions among the amino acids. The tertiary structure is essentially the three-

dimensional ‘packing’ of the secondary structures held together by interactions between the elements of the secondary structure.

Contrary to what might be expected given the vast number of possible configurations, proteins do not require extensive time to explore all these conformations. In fact, the folding process is relatively rapid, typically occurring on the timescale of microseconds to seconds for compact proteins, although the exact time can vary and sometimes be faster or slower [41], [42], [43]. However, it is important to note that not all functional proteins adopt a rigid, well-defined tertiary structure. Some exceptions, such as intrinsically disordered proteins (IDPs) like alpha-synuclein and tau, remain functional without a stable three-dimensional structure, illustrating the diversity in protein functionality [44], [45].

Protein folding is influenced by specific interactions between the amino acid residues in the protein, which help the protein avoid non-functional formations and reach its native structure more efficiently [41]. Proteins generally maintain thermodynamic stability in their native state, with their global minimum free energy being the lowest among all kinetically accessible structures [46]. Given the quick nature of protein folding, the idea of the funnel-shaped landscape has risen, which is believed to reduce the time it takes for proteins to achieve their native proper folded form. Unfolded proteins exhibit high enthalpy and entropy, while folded ones show the lowest values for both (Figure 4).

While the folding landscape offers numerous routes for protein folding, some of these pathways can lead to metastable misfolded states that are not energetically optimal [47], [48]. Misfolded proteins cannot function as they are supposed to; they may also malfunction or interact wrongly with other cellular molecules. However, cells employ various methods to prevent this, such as using molecular chaperones. Proteins are steered on the correct folding routes by chaperone

proteins, which shield them from disruptive interactions [49]. If proteins misfold, typically, chaperones intervene to help them fold correctly [50].

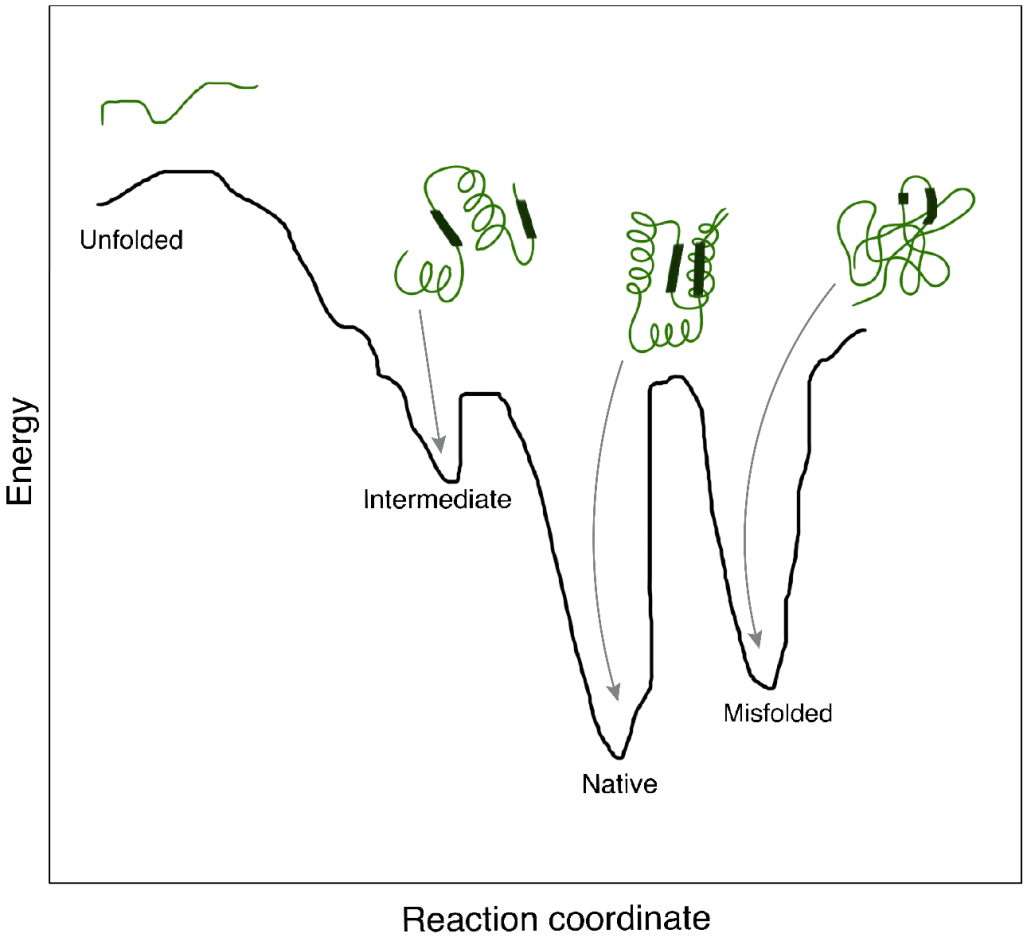

Figure 4. Notional cartoon of a one-dimensional energy landscape.

Additionally, cells have protease enzymes, which dismantle and eliminate misfolded proteins. These enzymes specifically catalyze the hydrolysis of peptide bonds, helping break down misfolded proteins [51]. However, complications arise when, with even these methods, the system cannot get rid of misfolded proteins. As mentioned before, certain diseases, like some specific cancers, Parkinson's, Alzheimer's, ALS, and type II diabetes, are linked to proteins that tend to misfold and bypass cellular defenses, resulting in persistent cell aggregates. Thus, improper

protein folding or the inability to maintain the correct form of folding results in disruption in biological systems, leading to an increased risk of diseases [50], [52].

1.4 Overview of the Thesis

The subsequent sections of the thesis are structured as follows. Chapter 2 delves into prion-like conversion and expounds on the role of SOD1 in the context of ALS in more detail. Chapter 3 describes the methodology employed to study prion-like conversion, highlighting how this technique enables precise observation of protein misfolding and subsequent propagation under mechanical stress. Additionally, this chapter describes the challenges encountered in the study of prion-like conversion of SOD1, providing a thorough discourse on the complexities involved. Furthermore, it introduces the design of our novel assay to monitor prion-like conversion and provides insight into the fundamentals of enzymology and the mechanisms underpinning data analysis. The thesis ends with the presentation of the final results of the investigation on several SOD1 mutants, delving into a discussion on the role of each mutant in prion-like conversion and revealing whether there is a meaningful relation between the rapidity of ALS progress in patients and the lag time observed for wt SOD1 conversion by different mutants.

Chapter 2: SOD1 and Prion-like Conversion

2.1 SOD1 Structure

The development of aerobic organisms capable of thriving in oxygen-rich environments necessitates a strong defense system against ROS, which are generated through the reduction of molecular oxygen by single electrons. While balanced amounts of ROS are advantageous for cell signaling and protection against pathogens, elevated ROS levels can harm cells, causing issues such as mutations, cell death, chromosomal abnormalities, and carcinogenesis. Furthermore, excessive ROS levels may contribute to the onset of numerous diseases, such as cancer, inflammation, diabetes, high blood pressure, and premature aging [30], [31].

SODs are the primary and most essential line of defense against ROS, specifically superoxide anion radicals [31]. They are found in all known forms of life, emphasizing their important function in biological processes [31], [53]. As mentioned in chapter 1, there are three isoforms of SODs in mammalian cells, one of which is SOD1 [31].

Copper-zinc superoxide dismutase1 or SOD1 is a metalloenzyme that catalyzes the redox reaction of superoxide anion to oxygen (O_2) and hydrogen peroxide (H_2O_2) at its active copper ion site by alternately transferring an electron to and from the superoxide radicals (Figure 5) [54].

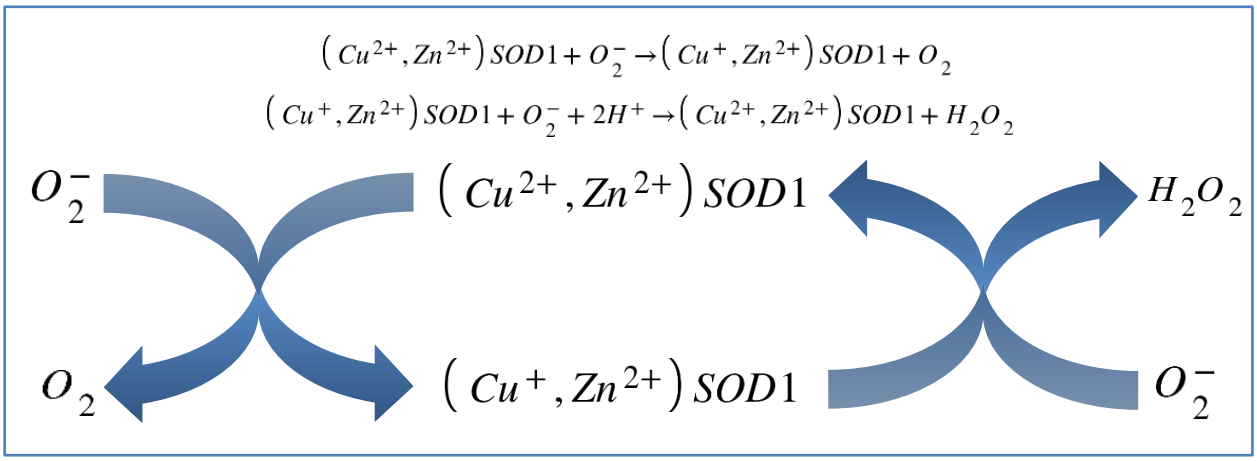

Figure 5. The enzymatic reaction of SOD1 with superoxide anion.

In the human body, SOD1 functions as a homodimer with a mass of 32kDa and comprises two identical subunits [55]. Each subunit includes 153 amino acids, organized into a beta-barrel structure consisting of eight anti-parallel beta-sheets and seven connecting loops [56] (Figure 6). Out of these seven loops, there are two loops, the “electrostatic loop” (residues 122-143) and the “metal binding loop”, also known as the “zinc loop” (residues 49-84), which are functionally vital. The electrostatic loop of SOD1 makes up about 11% of the protein’s exposed surface area and is composed of positively charged amino acids [57]. The remainder of the SOD1 exterior carries a negative charge, which leads to an electric field gradient that directs the negatively charged superoxide anions to the copper catalytic site [58]. The more positive charges in the electrostatic loop, the more catalytic activity of SOD1 due to the raising of the concentration of superoxide in the vicinity of the catalytic site [59].

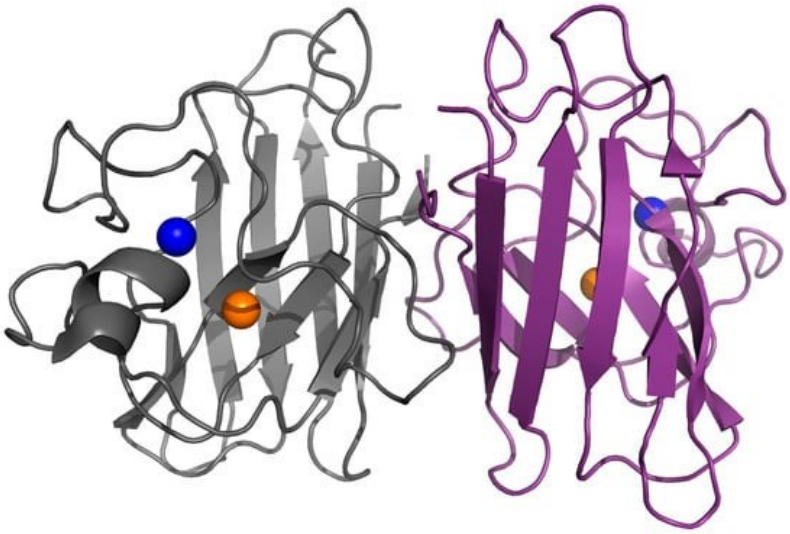

Figure 6. The structure of CuZnSOD1 protein in the human body. Human SOD1 is dimeric, and each subunit contains 153 amino acids, eight anti-parallel beta-sheets, seven connecting loops and two metal ions, copper, and zinc. This figure is adapted from [60].

The metal binding loop comprises residues crucial for the attachment of zinc ions [61], which plays a key role in SOD1 structural stability [62]. In each monomeric part of SOD1, a copper ion and a zinc ion attach to "beta bulges" along the protein strands. These metal binding sites are in proximity and are interconnected by a histidine residue (His63) and an additional bond (Asp124), which links to the copper ligand (His46) and the zinc ligand (His71). The binding of the copper ion is thought to be instrumental in the catalytic process. In contrast, the binding of the zinc ion plays a significant role in reinforcing the structural stability of the SOD1 enzyme. Each subunit of the SOD1 includes four cysteine residues: Cys6, Cys57, Cys111, and Cys146. The disulfide bond, a conserved feature, is crucial for the enzyme's stability and is formed between Cys57 and Cys146 [63]. Cys6 and Cys111 are not preserved across all species, and it is unique to only humans and great apes to have two free cysteine residues [64]. In the SOD1 structure, Cys6 is situated deep

inside the beta-barrel's core, and Cys111 is situated close to the interface where the dimer forms, which accounts for the high reactivity of Cys111.

2.2 SOD1 and ALS

The encoding function of the SOD1 gene produces the SOD1 proteins. In 1993, 11 different mutations in the SOD1 gene were found in 13 families dealing with familial ALS (fALS) [34]. Currently, more than 220 mutations of the SOD1 gene have been found in both familial and sporadic ALS cases [36], [65] (Figure 7). Around 50% of these mutations are recognized as disease-causative and have been identified in numerous families with a history of ALS or in several sporadic ALS cases. However, other mutations have only been identified in one family or a single individual with sporadic ALS; thus, their pathogenic classification is uncertain [66]. Various SOD1 mutants have distinct characteristics. From several hours to an entire day, the half-lives of SOD1 mutants may vary [67]. Different clinical phenotypes can be identified in patients carrying different SOD1 mutations. For instance, one group experiences a gradual progression of disease involving dysfunction in both upper and lower motor neurons, and the other group shows an aggressive progression with lower motor neuron dysfunction [68].

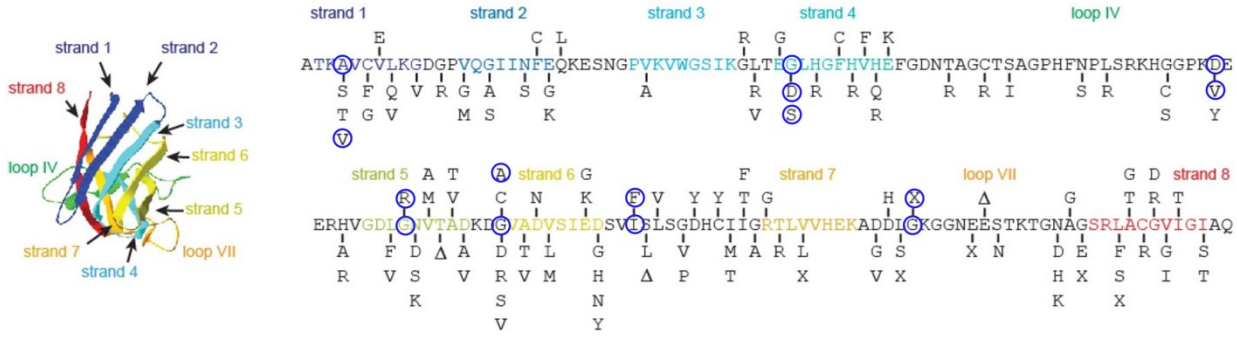

Figure 7. Structural mapping of AA sequence of SOD1 monomer with key mutation sites. Mutants that were investigated in this research are highlighted within dashed red boxes. This figure is credited to Michael Woodside.

Based on the mutations' position in the SOD1 protein structure, they can be classified into two distinct groups. The first group is categorized as metal-binding-region mutations, which are the mutations that occur within the SOD1 structure near sites where the metal ions bind, such as G85R, or within the zinc-binding loop, such as D125H. The ability of SOD1 to bind copper and zinc, which are the crucial elements for SOD1 structural stability and function, is significantly reduced by all the mutations in this group [69]. Typically, patients with the mutation in this group may experience more accelerated degeneration of neurons. Nonetheless, a notable exception is observed with the H46R mutation, which is associated with a considerably long survival time of about 17 years.

The second group is classified as beta-barrel or wild-type-like mutations located at sites distant from the metal-binding region, such as A4V, G41D, G41S, and G93A. Although these mutations generally do not impair the SOD1 protein's ability to bind metals, they may still destabilize the protein by affecting the dimer's stability or weakening the disulfide bonds, which are crucial for maintaining the integrity of the dimer interface. Patients carrying these mutations may experience milder symptoms and have a more positive prognosis. However, mutants like G93A or A4V present an aggressive disease course, with survival times ranging from one to three years, indicating their severity. These variations in clinical presentations among patients with the same category of SOD1 mutation suggest that, in addition to the mutation site, other contributing factors may influence the disease progression [61], [70], [71].

2.2.1 A Transition from “Functional Loss” to “Gain of Toxicity”

Initially, it was believed that the harmful impact of SOD1 mutations was due to a loss of SOD1 function to tackle oxidative stress, specifically its role in interacting with superoxide anions and turning them into oxygen and hydrogen peroxide. Indeed, a decrease in SOD1 activity to remove these anions was observed in several mutations, such as A4V, which was thought to lead to motor neuron degeneration [72], [73]. However, emerging evidence showed that some mutations associated with the disease only cause a slight reduction or no reduction at all in SOD1 enzymatic activity, which led to the gradual abandonment of the "loss of function" hypothesis [74].

There are some reasons for the “loss of function” concept to become less favored. Firstly, there is a significant contrast between the outcomes of SOD1 deficiency and SOD1 mutations, suggesting they have entirely different mechanisms for pathogenesis [75]. Secondly, the lack of a direct relationship between SOD1 activity and the progression of ALS also implies that SOD1 loss of function is not the primary reason for ALS [67]; finally, the survival rates of genetically engineered mice with a mutated version of SOD1 gene (while the rest of their genes have not been changed) do not show an extension when compared to a second group of genetically engineered mice that lack the SOD1 gene entirely [76]. Therefore, although “loss of function” may contribute to the disease to some extent, the majority of the toxicity of SOD1 in ALS is now believed to arise from a “gain of toxic function” due to misfolded protein variants.

2.2.2 Metal-Binding Impairment: A Way of SOD1 Mutant Gain of Toxicity

The initial toxic effect found in SOD1 mutations is associated with compromised metal-binding abilities, resulting in disrupted oxygen metabolism. SOD1 mutations can cause structural changes, leading to faulty binding with atypical substrates. For example, hydrogen peroxide (H_2O_2) may be turned into the highly reactive hydroxyl radical (OH^-) in fALS cases [77]. Moreover, another aberrant binding of SOD1 is with peroxynitrite ($ONOO^-$), which leads to the nitration of tyrosine residues within the SOD1 protein [78]. Mutations can cause SOD1 to lose its ability to bind zinc, leading to a reduction of copper in the structure of SOD1. This activity can reverse the enzyme's typical function, which results in the excessive production of superoxide anions [79]. The produced superoxide molecules react with nitric oxide, generating more peroxynitrite and intensifying the nitration of SOD1 tyrosine residues [54].

The reduced binding of metals by mutant SOD1 may also release copper and zinc ions, potentially contributing to neurotoxicity driven by these metals [80]. The specific role of altered copper chemistry and related oxidative reactions in ALS remains elusive. For instance, the increase of oxidation markers has been found in some ALS mouse models, while in others, it has not [81]. Additionally, the overexpression of wild-type SOD1 in some mice models with specific SOD1 mutants did not affect the disease's onset or progression [76], and elevated levels of wild-type SOD1 have been associated with an earlier onset of symptoms [82]. Deficiencies in SOD1 copper loading in mouse models, which result in decreased dismutase activity, developed motor neuron disease [83]. Also, mice with mutations in the copper-binding sites of SOD1 showed reduced enzyme activity and displayed ALS-like symptoms [84]. These findings collectively suggest that oxidative reactions triggered by copper contribute to some extent to the development of the disease mechanisms of ALS related to SOD1 mutations.

2.2.3 Misfolding and Aggregation: Another Way of SOD1 Mutant Gain of Toxicity

The other suggested ALS-related toxic effect of SOD1 mutations is that they induce the protein to lose its proper native fold, leading to protein misfolding and, in some cases, subsequent protein aggregation. The identification of SOD1-linked inclusions in motor neurons and supporting cells of the brain and spinal cord of ALS patients, ALS mouse models, and cells cultured with human SOD1 mutant gene indicates that protein aggregation is the characteristic feature of ALS linked to SOD1 [76], [85], [86]. The accumulation of misfolded or aggregated SOD1 has been found in various cellular compartments, supporting the idea that SOD1 misfolding and aggregation play a vital role in the pathogenesis of ALS.

The presence of SOD1 aggregates in the spinal cords of the ALS mouse model with specific SOD1 mutant indicates that the proteasome system's attempt to break these aggregates' structure is inefficient [87]. Mutant SOD1 can form aggregates with large molecular weights that may include soluble oligomers or insoluble aggregates by SOD1 itself or its interaction with other cellular materials; thus, it seems that misfolded SOD1 can avoid the biological breakdown pathways. In ALS mice models, soluble oligomers are detected in the early stages of the disease, while larger insoluble aggregates tend to occur at more advanced stages [61]. This indicates that soluble oligomers may be more toxic, while larger aggregates might result from other disease-related changes. The specifics of the aggregation process and their structure are unknown, although the SOD1 aggregation is a well-documented phenomenon [88].

2.3 Prion-like Behavior in SOD1

In prion disease, a native form of prion protein transforms into a misfolded, transmissible version of the prion protein. In other words, the misfolded prion protein directly interacts with the native form of the protein, converting it to a misfolded structure, thereby facilitating its own replication [2], [15], [16], [89]. This behaviour has been seen in some other proteins linked to some specific neurodegenerative diseases; the spread of misfolded proteins happens through a process akin to that seen in prion conditions, hence the term prion-like conversion. In this process, the misfolded proteins come into contact with natively folded proteins, causing them to take on the misfolding pattern (Figure 8). For SOD1 proteins, the evidence for prion-like conversion is still emerging.; however, an increasing amount of research shows that misfolded SOD1 proteins can pass information about their configuration to other natively folded SOD1 proteins, which aligns with the prion-like action [90], [91], [92]. It is worth noting that while SOD1 typically forms stable bonds that contribute to its structural integrity, when mutated, it can be more susceptible to becoming unstable and misfolded [90].

There are two mechanisms that have been suggested to explain process of prion-like conversion: First, template-directed misfolding, where the misfolded protein is actually more stable than the native form, but this stable state is only achieved through catalytic interaction with another misfolded protein; Second, nucleation- or seeded-polymerization, in which the misfolded monomer of SOD1 is initially less stable as a monomer but gains stability upon joining a multimeric aggregate [93].

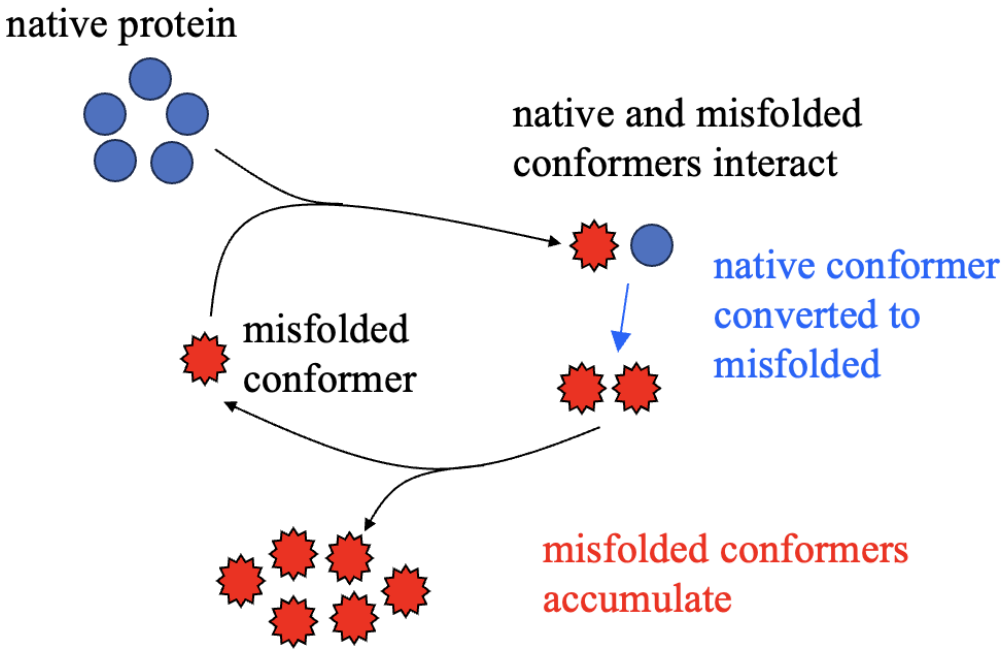

Figure 8. A cartoon illustrating prion-like conversion. In this process, misfolded conformers accumulate by interacting with natively folded proteins, converting them into misfolded structures.

According to a study [91], the template-directed mechanism is mostly responsible for the intracellular transformation of wt SOD1 into a misfolded form. This process starts when the encounter of wt SOD1 with overexpressed wild-type misfolded template causes a conformational change in the wt SOD1 structure. In this interaction the protein's solubility is maintained, therefore, it may be less prone to join aggregates in human cell lines [91]. This shows that similar to insoluble aggregates, misfolded but still soluble versions of SOD1 can induce propagated protein misfolding. Considering the native SOD1 is inherently stable in its homodimeric form and the observation that co-expression of wt SOD1 can help stabilize the mutant misfolded forms of SOD1 [94], [95], it is plausible to assume that the most likely candidate for undergoing misfolding

in this template-directed manner is newly synthesized wt SOD1, which has not yet reached its proper fold. However, this hypothesis still needs to be validated through experimental research [96].

Another mechanism observed in the prion-like conversion of SOD1 proteins, both in vitro and in cell culture, is seeded polymerization, also known as fibrillar aggregation. The likelihood of misfolded SOD1 proteins to aggregate is affected by specific mutations or other structural modifications [97] and is intimately linked to the protein's hydrophobic residues being exposed due to structural changes [98]. Patients' lifespan is impacted by the propensity of mutant SOD1 proteins to aggregate and their structural stability, both of which are important aspects in the development of diseases [99].

The process by which prion-like conversion happens for SOD1 mutants within the human body remains elusive. Therefore, developing a specialized assay that allows for detailed examination of structural alterations in wt SOD1 when in close proximity to a misfolded counterpart would significantly enhance our understanding of this complex phenomenon.

Chapter 3: Methodology

3.1 SOD1 Prion-like Conversion: Mechanisms and Limitations

The prion-like conversion mechanisms of SOD1 have not been broadly explored; however, a specific method has shed light on this phenomenon. This method, examining SOD1 prion-like conversion, is single-molecule force spectroscopy (SMFS), where optical tweezers are used to apply force between the ends of wt SOD1 monomer linked to a free-floating misfolded SOD1 mutant monomer via 50 amino acids long linker. This force destabilizes the heterodimer's structure, allowing the observation of how wt SOD1 at the close proximity of a misfolded mutant SOD1 unfolds and refolds in response to the applied load. The force-extension curves (FECs) generated by these unfolding and refolding events show the contour length changes associated with the unfolding of the protein, which is indicative of its native or misfolded states. The typical unfolding contour length of wt SOD1 provides a reference point for measuring deviations indicative of the influence exerted by the tethered misfolded SOD1 mutant. The method's strength lies in its ability to discern subtle changes in protein structure and directly observe the prion-like conversion process [100].

Research into the prion-like propagation of SOD1 faces notable limitations because there have been some challenges in studying this process. The misfolding process is a rare and transient phenomenon, complicating efforts to observe how misfolded conformers spread through a prion-like mechanism [101]. Additionally, with more than 220 mutants of SOD1 associated with ALS, each potentially affects the disease in its own way. This inherent variability adds complexity to the study, as it is possible that certain mutations might not directly engage in the prion-like conversion mechanism [102].

Nonetheless, these mutations could manifest diverse pathogenic roles, potentially affecting the trajectory of ALS. Determining the specific effects of each mutation underscores the importance of developing an assay capable of monitoring prion-like conversion across various SOD1 mutations. In this study, a distinctive method was developed to track the prion-like transformation of SOD1. This method involves tethering a misfolded SOD1 mutant monomer linked to ALS to a wild-type SOD1 monomer. Then, the activity of the wt SOD1 component is measured over time to observe its transition into an inactive, misfolded structure.

In heterodimer design, tethering the mutant to the wt SOD1 increases the effective local concentration of the misfolded protein within the assay while maintaining a low overall concentration, thus distinguishing the conversion process from aggregation. Notably, the heterodimer features an unstructured and relatively long tether composed of 50 amino acids, equivalent to approximately 18 nm in contour length. This tether incorporates glycine and serine, which are commonly selected for the flexible linkers in engineered proteins with multiple domains [103], [104]. The amino acid sequence of this linker is:

GSGGSGSGGSGSGGSGSGGSGSGGSGSGGSGSGGSGSGGSGSGGS

Our initial attempts with a 15 amino acid tether proved insufficient, as it restricted the misfolded structure's ability to induce conversion. Subsequently, the extended 50 amino acid tether was employed, leading to improved outcomes. Nonetheless, determining the optimal tether length remains a largely uncharted area of our research. The current design of the tether aims to minimize restrictions on the interaction between the two domains, thus enhancing the accuracy of observations regarding the wt SOD1 conversion process (Figure 9).

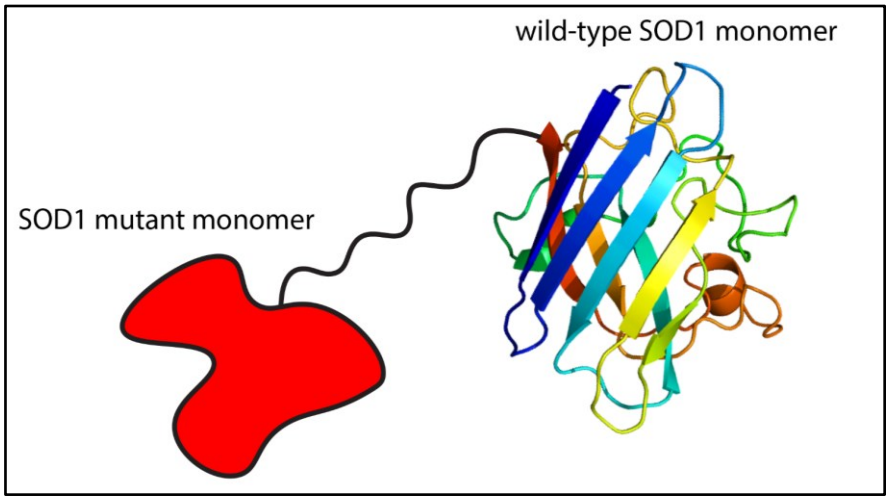

Figure 9. SOD1 heterodimer construct design. This diagram depicts the engineered heterodimer comprising a wt SOD1 monomer and a mutant SOD1 monomer tethered with a 50 amino acids long tether.

3.2 Protein Preparation

3.2.1 Protein Expression

In the course of this study, plasmids encoding the specific SOD1 mutant genes under investigation were purchased from GeneScript. This acquisition ensured access to high-fidelity genetic sequences essential for the integrity of this research.

Firstly, the heterodimer protein composed of wt SOD1 monomer and the mutant SOD1 monomer was recombinantly expressed in *E. coli* (bacteria) strain BL21 (DL3). Then, the bacterial sample was cultured by being spread over the surface of an agar plate with an ethanol-sterilized spreader and plates were covered and kept in the incubator at 37°C overnight, letting the bacteria colonies grow. In the next stage, a single colony of bacteria was selected to be cultivated in a liquid Lysogeny broth (LB) medium containing 100 µg/ml of ampicillin and 34 µg/ml of chloramphenicol. This mixture is then incubated at 37°C and agitated at a speed of 225 rpm

throughout the night. The next day, the mixture was centrifuged in 50 ml bottles at 5100 g for 10 minutes at 20℃ in a Beckman Allegra 25R bench-top centrifuge. The remaining supernatant was discarded, and the precipitated cells were resuspended in 10 ml of fresh LB medium and then transferred to a larger 2 L culture for growth and incubation at 37℃ and 225 rpm. The cultivation of colonies involves regular measurement of the optical density at 595 nm (OD595 nm).

Upon reaching an OD595 nm value between 0.5 and 0.7, the time during which cell growth and division occur at their most rapid and robust rate, the induction of SOD1 was initiated by the addition of isopropyl-β-D-thiogalactopyranoside (IPTG) to reach 1 mM final concentration. After induction, the culture grew between 16-20 hours, and then *E. coli* cells were harvested by spinning them at 5100 times gravity for 12 minutes at 4℃ in 500 ml bottles using a Beckman Allegra 25R refrigerated bench-top centrifuge.

The last step of protein expression is to resuspend the cell pellets, per 500 ml culture, in a resuspension buffer containing 40 ml SOD1 equilibration buffer (50 mM Tris, pH 7.5, 50 mM NaCl, 10 mM $MgCl_2$, and 40 mM or 25 mM imidazole), 1 µl hen egg white lysozyme (HEWL), 2 µl deoxyribonuclease I (DNase I), and one tablet complete EDTA-free protease inhibitor cocktail. Hen egg white lysozyme (HEWL) serves as a vital enzyme for the degradation of bacterial cell walls [105]. DNase I is included to decompose genomic and plasmid DNA, which otherwise would increase the viscosity of the preparation [106]. The protease inhibitor tablets play a crucial role in blocking the function of proteases, which are enzymes that cause the breakdown of proteins [107]; since these tablets do not contain EDTA, they do not hinder metalloproteinases. The last step of this stage is to store the resuspended pellets in a -80℃ freezer.

3.2.2 Protein Purification

The next step for preparing a suitable SOD1 protein sample involves the process of protein purification. Initially, bacterial pellets are retrieved from storage at -80°C and thawed. The mixture is then subjected to sonication in an ice bath using a Branson sonicator at six cycles of 10 seconds each at 65% power output and duty cycle between 60% to 70%, with a resting period of 30 seconds on ice between cycles. The purpose of sonication is to disrupt any cells that were not already broken down by the lysozyme and to fragment the residual genomic DNA present in the lysate, thereby decreasing its viscosity. Following sonication, the sample was put in heavy-walled centrifuge tubes and spun in a Beckman Allegra 25 R centrifuge using a JA-14 rotor at 14000 rpm for 90 minutes at 4℃. The pellet was thrown away, and the supernatant was kept and passed through a 0.45 μm syringe filter to ensure that the remaining particulate matter was eliminated and prepared for the next step of column chromatography.

The next step is to prepare the AKTA Purifier and Ni-immobilized metal affinity chromatography (Ni^{2+}-IMAC) column by cleaning all equipment lines with specific buffers. First, the ends of all four lines, A1, A2, B1, and B2, were put in fresh MilliQ water, and the process of cleaning started by selecting the MANUAL mode, then the PUMP, and navigating to the PUMP WASH PURIFIER option, followed by choosing lines A1, A2, B1, and B2 to be washed out and then EXECUTE. Next, lines A1 and A2 were put in the SOD1 equilibration buffer (Buffer A), and lines B1 and B2 in the SOD1 elution buffer (Buffer B), and again, the PUMP WASH PURIFIER option was selected. The actual washing of the lines on the AKTA system is done in PAUSE mode, whereas all other operations are done in RUN mode. Then, the proper column was installed in position 8 for subsequent procedures.

Next, the INJECTION VALVE needs thorough cleaning since it is the pathway for the protein sample on its way to the column and the fraction collector. This process started by selecting the MANUAL mode, then in the PUMP, choosing SAMPLE FLOW-960 with a FLOW RATE of 5 ml/min, then selecting OUTLET VALVE and changing it to F2. In FLOWPATH, INJECTION VALVE was changed to INJECT, and the specified solution went through the system for 10 minutes, then changed the INJECT to LOAD and waited for 5 minutes. The system was washed out with MilliQ water, 1M NaOH, MilliQ water,0.1N HCl, and MilliQ water, respectively.

The next step is to regenerate the Ni^{2+}-IMAC column. In this part, the old nickel ions are stripped and replaced with new ones, which helps remove any proteins that have bound in previous purifications. In this process, all the selections are the same as the cleaning INJECTION VALVE step; the difference is that in the FLOWPATH part, INJECTION VALVE changes to INJECT, and there is no need to change to LOAD also, COLUMN POSITION needs to change to the position 8, and for each solution, 5 column value (25 ml), passing through the nickel column is enough. The solutions used in this step are 50 mM EDTA, MilliQ water, 50 mM NiSO4, MilliQ water, and SOD1 Equilibration Buffer. EDTA solution removes the Ni^{2+} ions efficiently, as the color change in the column from blue to white indicates the completion of Ni^{2+} removal. After the column has been stripped, it must be thoroughly rinsed to eliminate all EDTA traces to allow efficient resin reloading, so the column was washed with MilliQ water. Next, by passing through the NiSO4 solution, the column color turns to a greenish blue, indicating the completion of nickel loading. Following this, to clear any surplus Ni^{2+} from the column, it stabilized with a brief MilliQ rinse, and then the equilibration buffer went through the column (Figure 10).

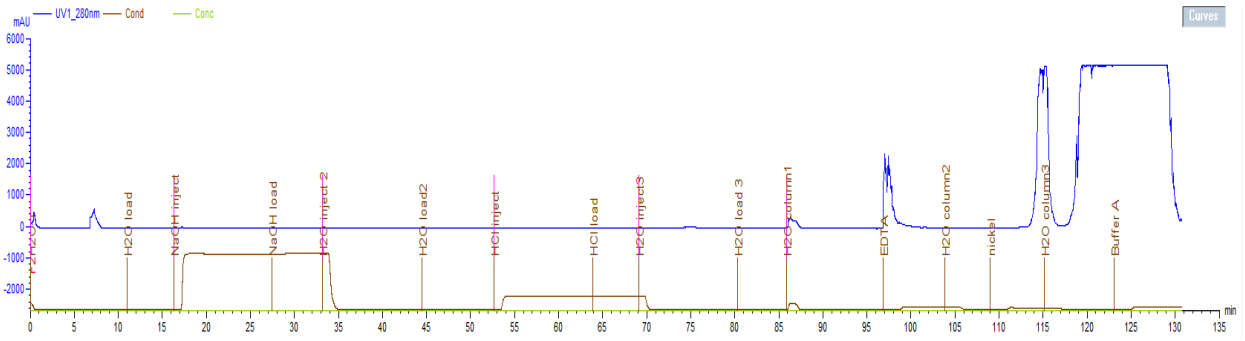

Figure 10. The chromatogram of the cleaning process of the AKTA purifier

Now, the AKTA purifier is ready for protein purification. At this stage, the protein sample was first loaded into the column at a flow rate of 2 ml/min with the SAMPLE PUMP. When proteins are going through the nickel column because of their specific engineered structure that is attached to six histidine amino acids, which have a high affinity for nickel, they bind to the nickel ions on the column beads. Then, any unbound proteins are washed away using the equilibration buffer until the UV absorbance at 280 nm returns to baseline levels; this step usually takes 15 to 20 minutes. The subsequent phase involves eluting the target protein, which is His6-tagged SOD1 dimer, using an adequate volume of elution buffer (Tris-Cl 50 mM pH 7.5, NaCl 150 mM, $MgCl_2$ 10 mM, $CaCl_2$ 1 mM, imidazole 600 mM). Imidazole has a high affinity for nickel ions; therefore, during the elution step, attached proteins compete with imidazole molecules to bind to the nickel. Due to the high concentration of imidazole in the elution buffer, imidazole molecules displace the proteins, causing the proteins to elute from the column and be collected in fractions.

3.2.3 SDS-PAGE

The next step is to evaluate the purification quality with sodium dodecyl sulphate–polyacrylamide gel electrophoresis (SDS-PAGE). SDS-PAGE is a method used to separate and identify proteins in a mixture by their molecular weight. This technique involves denaturing proteins using a detergent and heat and then running them through a polyacrylamide gel. The proteins are sorted by size as they move through the gel, with the smaller molecules travelling faster. The gel consists of two layers with different acrylamide concentrations: a lower percentage of stacking gel for the initial organization of proteins and a higher percentage of resolving gel for detailed separation. Typically, a 12% gel is used for a broad range of proteins (Table 2), but this percentage can be adjusted to better resolve either larger or smaller proteins, depending on the need.

The 1.0 mm spacer glass plates were initially washed and set up in the casting stand. Then, the components for the resolving gel were mixed and poured between the gel plates until it reached a point 2 cm beneath the top edge of the shorter plate or in another way, a volume of 4.3 ml of resolving gel can be pipetted between glasses, then 70% ethanol was added on top to remove any residual SDS and surface bubbles, and also flatten the meniscus along the edges. After about 30 minutes, that resolving gel solidified, ethanol was decanted, plates were washed carefully, and a small piece of filter paper was used to dry between plates well. The stacking gel was prepared while waiting for the resolving gel to solidify. TEMED, which accelerates the gel's solidification, was added just before layering the stacking gel atop the resolving gel. To form the wells, a 1 mm, 10-well comb was carefully inserted between plates while adding the stacking gel, which was filled to the upper edge of the shorter plate. Vigilance was exercised to avoid any air bubbles within the wells, and the gel was left undisturbed to set.

Resolving gel 12% (10 ml for 2 mini gels)		Stacking gel 4% (5 ml for 2 mini gels)	
Reagent	Volume	Reagent	Volume
MilliQ H_2O	4.3 ml	MilliQ H_2O	3.8 ml
1.5M Tris-Cl pH 8.8	2.5 ml	1.0M Tris-Cl pH 6.8	0.63 ml
Acrylamide/bis-acrylamide 40% (29:1)	3 ml	Acrylamide/bis-acrylamide 40% (29:1)	0.5 ml
SDS 10%	100 µl	SDS 10%	50 µl
Ammonium persulphate (APS) 10%	50 µl	Ammonium persulphate (APS) 10%	25 µl
TEMED	5 µl	TEMED	5 µl

Table 1. The solutions required for making SDS PAGE

Now, it is time to run the gel. First, 6X Sample Buffer (6XSB) dye was mixed with the protein at a 1:5 ratio (usually 2 µl of 6XSB and 10 µl of the protein). The mixture was then placed in a 95℃ water bath to boil, undergo further denaturation, and centrifuged for 3 minutes. Upon the completion of polymerization of the gel, the combs were carefully removed, and the wells were created. The gel assembly was then securely positioned within the Mini-Protean II electrophoresis apparatus. Subsequently, the 1X running buffer was methodically added to both the upper and lower chambers. Any air bubbles that emerged because of the comb removal were meticulously eliminated by delicately pipetting the running buffer into each well, ensuring an unobstructed path for the samples during electrophoresis.

For each gel, 2 µl of the molecular weight ladder (MWT) was added into the first well, and then the rest of the wells were filled by the sample-protein mix using gel-loading tips. Electrophoretic separation commenced at an initial voltage of 100 V to facilitate the penetration of the dye into the gel matrix, a process which spanned approximately 30 minutes. Subsequently, the voltage was elevated to 150 V, propelling the dye front toward the gel's base over an hour. Upon completion of electrophoresis, the assembly was meticulously dismantled, and the gel, now separated from the spacers and glass plates using a specialized plastic tool, was placed in a water-filled plastic container to relax briefly. Afterward, the water was decanted, and the gel was submerged in Coomassie Blue G250 staining solution on an orbital shaker overnight. The subsequent day entailed the removal of the stain, a thorough rinse of the gel in water for an extended duration, and a final comparison of the resolved protein bands against a standard molecular weight marker.

3.2.4 Protein Dialysis

When the protein quality is verified, and the fractions containing the purest proteins are identified, it is time to dialyze the protein. The dialysis process commenced to remove excess imidazole and replace it with a sodium phosphate buffer. In this stage, first, the selected fractions were pooled, then the dialysis membrane, with a molecular weight cut-off (MWCO) of 12000-14000, was prepped by rinsing and securing one end with a clamp, then carefully loaded with the protein mixture, ensuring space for expansion before sealing the other end. After clamping and filling it with the protein solution, it was placed in 4 L of sodium phosphate buffer (100 mM, pH 7.0) to incubate overnight at 4°C with gentle stirring. The following day, a fresh dialysis buffer was made, the protein was placed in it, and the solution was left to incubate for another day.

Post-dialysis, protein concentration was gauged and, if necessary, concentrated via centrifugation to eliminate the extra buffer and increase the concentration. A spectrophotometric analysis was conducted to quantify the protein concentration. An aliquot of 200 µl of the protein's dilution buffer was transferred into a cuvette to establish the baseline absorbance in the spectrophotometer. Following this calibration, the absorbance of a 200 µl protein sample was measured at a wavelength of 280 nm. The protein concentration was deduced using the Beer-Lambert law, $A = \varepsilon lc$, where A denotes absorbance, ε is the molar extinction coefficient, l represents the cuvette's path length set at 1 cm, and c is the concentration [108]. The protein's concentration was calculated with the absorbance recorded and the extinction coefficient known. Upon ascertaining the protein concentration, aliquots were prepared and stored at -20°C for subsequent analysis.

3.3 Microplate Reader

The microplate reader, a staple in contemporary biological, biochemical, and biophysical research, offers a high-throughput analytical approach to concurrently assay multiple samples. This device can detect a range of events within the wells of a microtiter plate. A microplate reader is equipped with numerous wells, each capable of containing up to 200 µl of a sample solution. The standard configuration for these plates is the 96-well format, arranged in a 12×8 matrix. Biochemical reactions occur within these wells, and the microplate reader's role is to measure and analyze these reactions quantitatively. It does so by detecting and interpreting the optical properties of the samples, which could include light signals emitted from them. The detections and interpretations vary depending on the specific reaction conditions and the constituents of each

well. This instrument offers several operational modes, with the most prevalent being absorbance, fluorescence, and luminescence.

In the context of this research, the absorbance mode was utilized to track changes in absorbance that occur during the prion-like conversion of SOD1. This process is initiated by directing a beam of light of a precise wavelength, 450 nm in this instance, chosen due to the presence of water-soluble tetrazolium (WST-1) dye in the SOD1 assay towards the sample. This wavelength selection is achieved through the application of a monochromator. On the opposite side of the well, a photodetector gauges the quantity of light that passes through the sample, establishing a relationship between the transmitted light and the concentration of the target molecule within. This critical measurement, known as the optical density (OD) or absorbance, is then calculated by the instrument's software using the formula:

$$A_\lambda = \log_{10}(\frac{I_0}{I})$$

I denotes the intensity of the light that has passed through the sample at the specified wavelength λ, and I_0 represents the intensity of the light before interacting with the sample [109]. Throughout the course of this experiment, absorbance readings were taken at 5-second intervals over a span of 60 seconds. These readings were integral to the subsequent analyses that sought to elucidate further the characteristics and behaviour of the prion-like conversion of SOD1.

3.4 SOD1 Activity Assay Solution

The most crucial factor influencing the biological efficacy of antioxidant enzymes lies in their activity; therefore, enzymatic assays are utilized to assess the true functional capacity of antioxidant enzymes [30]. The SOD1 activity can be measured using various assays, including colorimetric assays. The assay used in this study works based on the change of concentration of a colorimetric reagent WST-1 in the protein solution [110].

Solution	Final concentrations	Volume
BSA-DETAPAC mixture	1 mM DETAPAC, 0.13 mg BSA	12.9 ml
Catalase 40 U/ml	1 U	0.5 ml
Xanthine 1.18 mM	100 μM	1.7 ml
WST-1	56 μM	0.5 ml
Potassium Phosphate Buffer (PB)	50 mM	0.3 ml
BCS 10 mM	50 mM	0.1 ml
Total volume	–	16.0 ml

Table 2. The materials required for making SOD1 activity assay.

This assay uses xanthine and xanthine oxidase to generate superoxide anions, with WST-1 reduction serving as the indicator for anion production. Competition for superoxide anions occurs between WST-1 and SOD1 heterodimers, with increased WST-1 reduction indicating

diminished SOD1 activity. Over time, as SOD1 undergoes prion-like misfolding, its activity decreases, allowing a higher amount of WST-1 oxidation and a resultant yellow color from forming WST-1 formazan (Figure 11). This shift in color correlates with the progression of SOD1 misfolding (Figure 12).

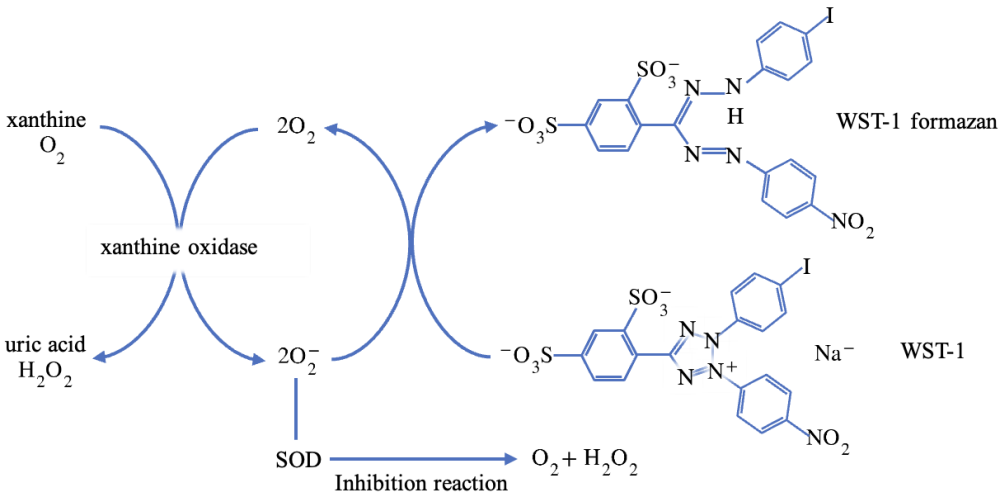

Figure 11. Diagram of the SOD1 activity assay. Xanthine and xanthine oxidase catalyze the production of superoxide anions. A competitive reaction ensues between SOD1 and WST-1 for superoxide anions. The subsequent conversion of WST-1 into WST-1 formazan, observable as a colorimetric change, inversely indicates SOD1 activity through its superoxide anion inhibition reaction.

To facilitate this study, a heterodimer construct combining a misfolded SOD1 mutant with a wild-type monomer was used. The assay was designed to monitor the wild-type component, specifically focusing on detecting reduced enzymatic activity, a marker of prion-like conversion of the wild-type domain. But it should be noted that there is a possibility that the misfolded SOD1 mutant retains its own enzymatic activity, potentially up to levels comparable to the wild-type

SOD1. Consequently, the absence of a detectable reduction in overall SOD1 activity may not definitively indicate a lack of conversion within the wild-type domain.

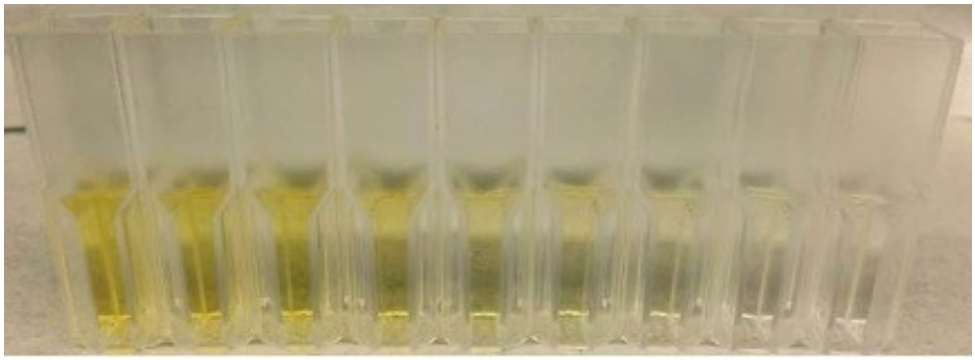

Figure 12. SOD1 assay colorimetric transition indicative of SOD1 conversion. Color change in the SOD1 activity assay correlates with prion-like conversion. The assay's increasing yellow intensity signifies more WST-1 oxidation, indicating a decrease in SOD1 activity due to its conversion to a misfolded state.

Catalase was added to eliminate the generation of any hydrogen peroxide as the product of the enzymatic activity of SOD1, while bovine serum albumin (BSA) was used to prevent bathocuproinedisulfonic acid (BCS) precipitation. BCS and Diethylenetriaminepentaacetic acid (DETAPAC) were employed to inhibit iron-dependent oxidation and radical formation. The sequential introduction of assay reagents is crucial for accuracy. The assay was conducted under mildly denaturing and reducing conditions to expedite the misfolding process. Enzymatic activity quantification was achieved by measuring the absorbance of the formazan dye at 450 nm, with the rate of dye production being directly proportional to the activity of SOD1.

The preparation of protein samples for the SOD1 activity assay entails the use of Tris(2-carboxyethyl)phosphine (TCEP) at a concentration of 500 mM, Guanidine hydrochloride (GuHCl) at 6 M, and a 100 mM sodium phosphate buffer with a pH of 7.0. The protein solution is utilized at a final concentration of 25 µM. Three replicates of each protein sample were prepared and placed in an incubator at 37°C, shaking at 300 rpm. For measurements, samples were removed from the incubator, and 2 µl were diluted with 98 µl of potassium phosphate buffer. The diluted samples were then allocated into a 96-well plate configured with a 2×3 (2 rows and 3 columns) matrix for the plate reader: the first row for PB buffer as control and the second for protein samples, each well receiving 20 µl.

Upon initial use at time zero, the plate reader's dispensers were washed with MilliQ water, with subsequent priming of 1 ml of the assay and XO solutions. Before each reading, the dispensers were primed with 100 µl to 300 µl of the assay and XO solutions. Measurements were conducted using Gen5 software, with absorbance readings taken at the 450 nm wavelength corresponding to the absorption peak of WST-1. For each measurement, 160 µl of activity assay reagent and 20 µl of XO solution were dispensed into each well, with absorbance measurements recorded at 5-second intervals over a period of 60 seconds.

3.5 Data Analysis

After the measurements, the graph of absorbance vs time of both three control wells and three protein samples was plotted (Figure 13A) and based on the best-fitted curve, the average slope of the three control graphs was calculated. The calculated number indicates the average rate of superoxide reduction by the WST-1 in the absence of SOD1, so this is the baseline reaction rate without any enzymatic inhibition. The slope of the fitted curve on absorbance vs time graph of the

protein measurements shows the rate of superoxide reduction in the presence of SOD1. Therefore, the slope of the mentioned graph for protein solutions indicates the activity of SOD1 in competing with WST-1 to react with superoxide. At the first hours of the experiment, wt SOD1 is active and is able to reduce more superoxide itself, leaving less for the WST-1 to reduce, resulting in a lower slope compared to the control. By passing time, more native SOD1 converts, leaving more for the WST-1 to reduce, so the slopes of fitted curves on control and protein graphs are closer to each other. Therefore, the significant difference between the control and protein slopes indicates the effective inhibition of SOD1; conversely, the slight difference between control and protein slopes suggests the low activity of SOD1 or the conversion of native SOD1 to its misfolded counterpart. After determining the slopes, the percentage of relative inhibition of superoxide anion reduction was calculated using the formula:

$$\%\, Inhibition\ of\ O_2^-\ reduction = \frac{Control\ rate - Protein\ rate}{Control\ rate} \times 100$$

This calculation serves to normalize SOD1 activity to the control condition. By adopting this approach, the influence of SOD1 on the reaction is isolated, effectively eliminating any nonspecific background activity. Such normalization is crucial for precisely quantifying SOD1's specific activity, ensuring that the observed effects directly relate to the enzyme's functional impact within the experimental setup.

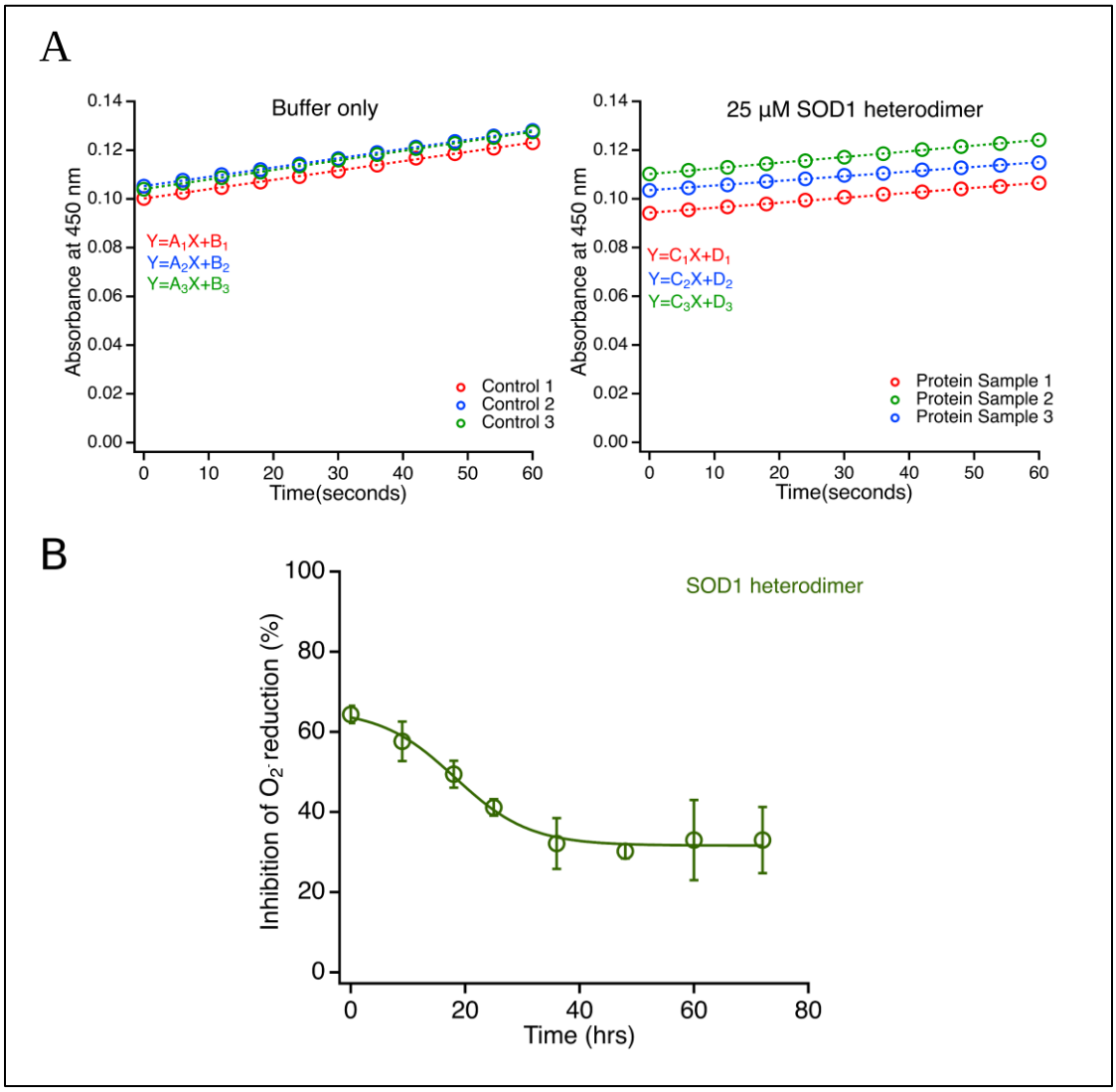

Figure 13. Summary of data analysis from initial raw data to the final enzymatic activity curve. A) Absorbance values for buffer controls and protein samples plotted against time. The slope of the fitted curves is used to determine the percent Inhibition of O_2^- reduction at specific time points. Also, standard error of the mean (SEM) is calculated for the triplicate protein samples. B) Final plot of percent Inhibition of O_2^- reduction versus time, illustrating the enzymatic activity of the SOD1 mutant under investigation.

Upon completion of the experimental phase, data analysis was conducted using Igor Pro 9 software. This involved plotting the percentage inhibition of superoxide anion (O_2^-) reduction against time (Figure 13B). The observed data trends on some of these plots were best modelled using a sigmoidal curve, described by the general formula:

$$A = A_0 + \frac{A_{max}}{1 + \exp(-\frac{t - t_{1/2}}{\tau})}$$

In this model, A represents the percentage inhibition of O_2^- reduction, and t denotes the time. Parameter A_0 refers to the initial percentage inhibition value at the start of the time course. A_{max} indicates the maximal change in A from its baseline value. $t_{1/2}$, or 'time one-half,' represents the time at which the function achieves half of its maximum change. The parameter τ characterizes the steepness of the curve, reflecting the time scale over which the response variable A transitions from the baseline to the maximum change. A smaller τ value indicates a sharper transition, whereas a larger τ results in a more gradual change. In certain instances, the data conformed to a pattern where a linear model with a zero slope ($A=A_0+A_1t$, where $A_1=0$) was the most appropriate fit.

Chapter 4: Results and Discussion

This research aimed to develop a simple and scalable ensemble assay for observing prion-like conversion of wt SOD1 by SOD1 mutants associated with ALS. To achieve this, a series of experiments were designed, which included a) the purification of SOD1 heterodimers to ensure a reliable supply of the target proteins and b) the utilization of microplate reader technology to track the progression of the prion-like conversion process. The findings from these investigations are compiled and detailed within this chapter.

4.1 Purification Results

The initial phase of assessing the prion-like conversion process involved the purification of the proteins of interest, which were wt-G85R, wt-G127x, wt-A4V, wt-I104F, wt-G41D, wt-D76V, wt-G93A, and wt-G41S heterodimers. The goal was to determine an optimal purification protocol yielding the highest purity for each heterodimer. This pursuit necessitated multiple purification trials for selected heterodimers, focusing on optimizing the imidazole concentration in the equilibration and elusion stages. Imidazole's role is critical as it competes with the His-tagged SOD1 heterodimers for binding sites on the nickel affinity column.

Imidazole concentration in the equilibration buffer required optimization to ensure that this concentration was not excessively high, which might result in the desired His-tagged proteins being inadvertently washed away along with non-specifically bound molecules. Conversely, too low a concentration might fail to displace non-target particles, compromising the purity of the protein. To refine the purification protocol, the imidazole concentration in the equilibration buffer was varied, alongside adjustments to the duration and method of the wash steps. Gradient and

constant equilibration strategies were explored to determine the most effective purification approach for each SOD1 heterodimer.

The chromatogram of the SOD1 heterodimer wt-A4V (Figure 14A), wt-I104F (Figure 15A) and wt-G41S (Figure 16A) illustrates the protein loading phase, which persisted for approximately 19 minutes. The elevated absorbance at 280 nm (UV1_280 nm) during this phase is attributable to the intrinsic light absorption properties of the tryptophan (Trp) and tyrosine (Tyr) amino acid residues at this wavelength. A substantial absorbance peak was observed, indicating the passage of a considerable concentration of proteins through the chromatography column. This was followed by a reduction in UV1_280 nm absorbance, corresponding to the equilibration stage. During this stage, unbound proteins and other particles were washed from the column using a buffer containing 40 mM imidazole and 10% elution buffer. The decrease in UV1_280 nm suggests the successful removal of these unbound components, which took approximately 20 minutes to reach a baseline comparable to the starting conditions, signifying column clearance. Subsequently, the elution phase was initiated by increasing the imidazole concentration and introducing 100% elution buffer, resulting in a discernible peak, indicating the release of bound proteins from the column. The collection phase was completed in approximately 10 minutes, yielding nine fractions.

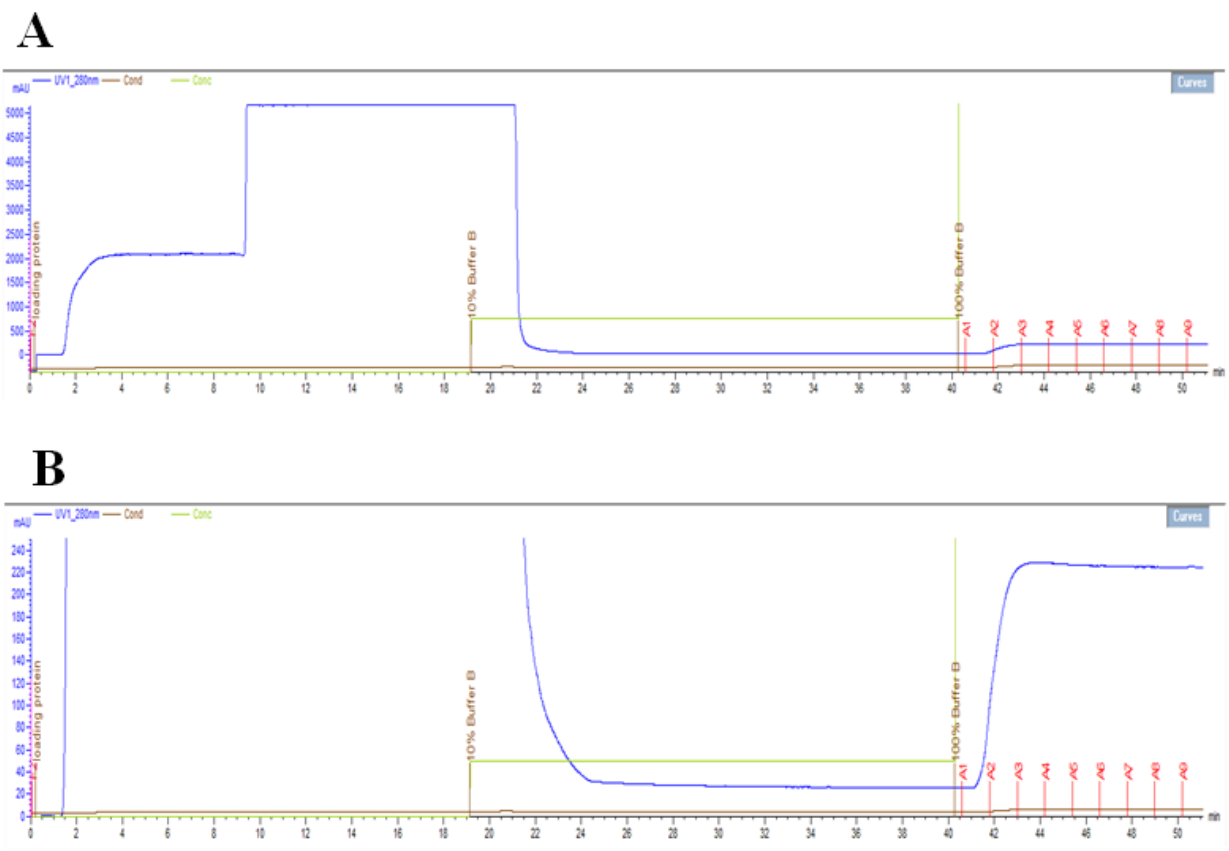

Figure 14. The chromatogram of the SOD1 heterodimer wt-A4V. Part A) depicts the entire chromatographic sequence, including protein loading, equilibration, and elution phases. Part B) provides a magnified view of the equilibration and elution stages with an adjusted scale for enhanced detail.

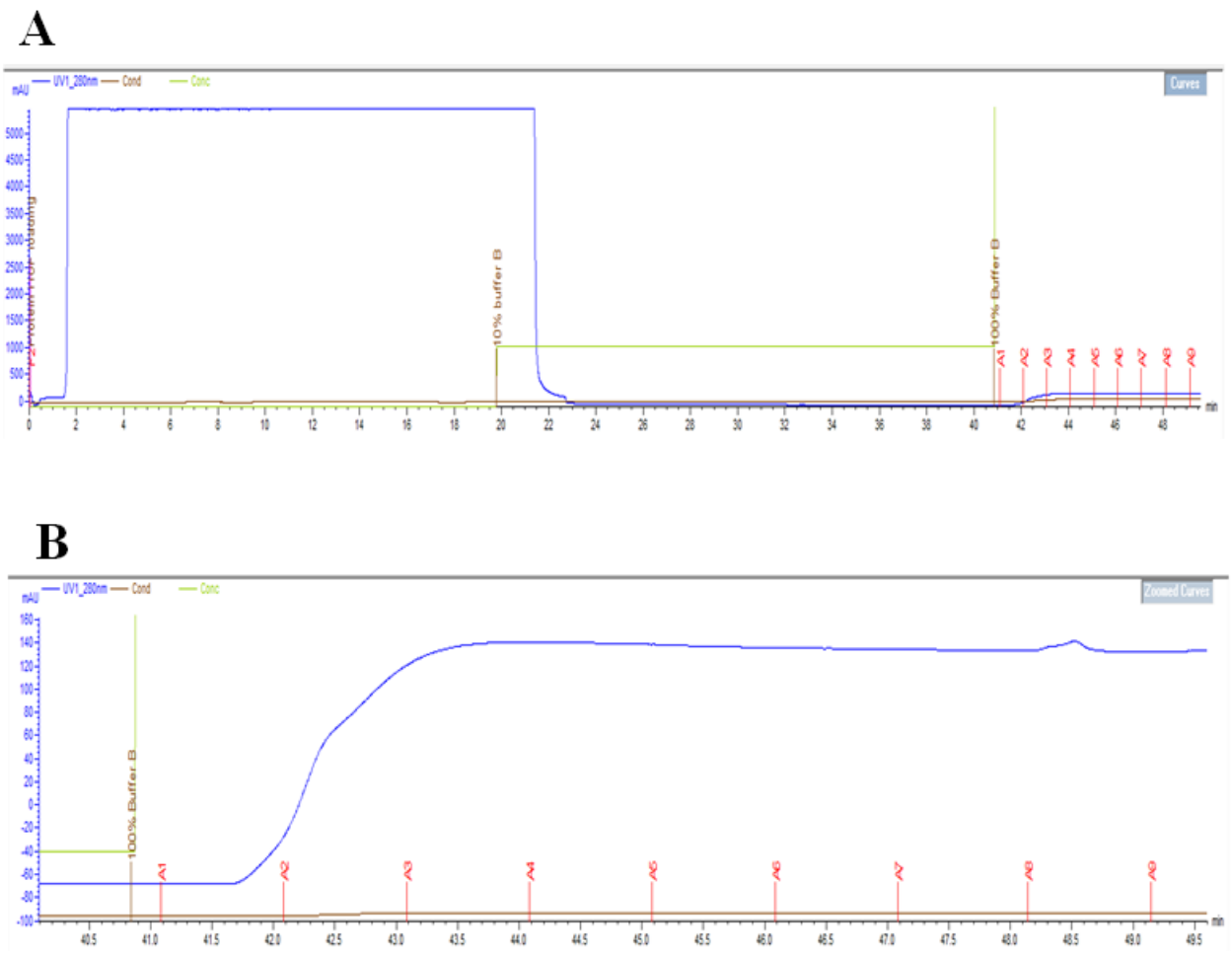

Figure 15. The chromatogram of the SOD1 heterodimer wt-I104F. Part A) illustrates the full chromatographic process. Part B) zooms in on the equilibration and elution phases, with the scale refined to improve the clarity of the details.

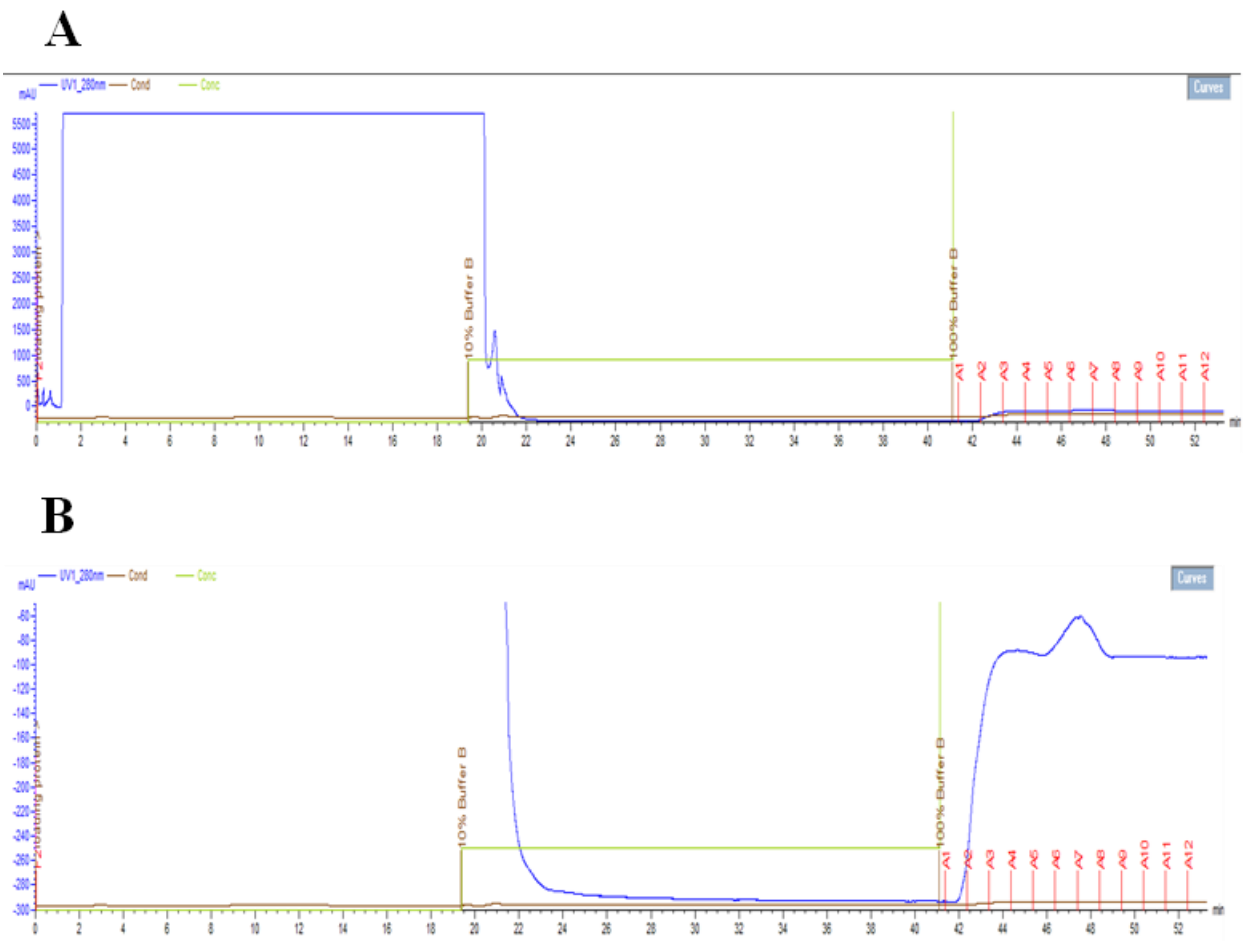

Figure 16. The chromatogram of the SOD1 heterodimer wt-G41S. Segment A) presents the complete sequence of chromatography. Segment B) offers a detailed examination of the equilibration and elution phases with a modified scale to highlight finer aspects.

Chromatographic profiles of SOD1 heterodimers, including wt-G41D, wt-G93A, wt-D76V, wt-G127X, and wt-G85R, are presented in Figures 17A, 18A, 19A, 20A, and 21A, respectively. The duration of the protein loading phase varied, extending from 20 to 35 minutes, depending on the targeted protein purification volumes. Pronounced peaks in the UV absorbance at 280 nm were recorded, signifying the transit of proteins through the column at significant concentrations. These peaks then diminished in intensity, marking the equilibration phase, where conditions were optimized for each protein variant to ensure maximum purification efficiency. Specifically, an equilibration buffer of 40 mM was employed for wt-G41D, wt-G127X, and wt-G85R, while a 25 mM buffer was utilized for wt-G93A and wt-D76V. The equilibration stage incorporated the equilibration buffer and the 5% to 10% elution buffer and varied in duration from 10 to 45 minutes until UV absorbance baselines were restored to initial levels, denoting the successful elution of non-specifically bound substances.

During the elution phase, strategies were tailored to each protein to achieve optimal separation; for wt-G41D and wt-G93A, a linear gradient reaching 100% elution buffer was applied over a period of 10 minutes. In contrast, wt-G85R and wt-G127X experienced an immediate introduction to a full-strength elution buffer, bypassing a gradient. Meanwhile, wt-D76V's elution commenced with a 50% buffer gradient over 10 minutes, followed by an abrupt shift to 100% elution buffer. The collection of the purified proteins, delineated by these distinct elution methods, was accomplished within a timeframe of 10 to 20 minutes. SDS-PAGE subsequently assessed the purity of the eluted proteins.

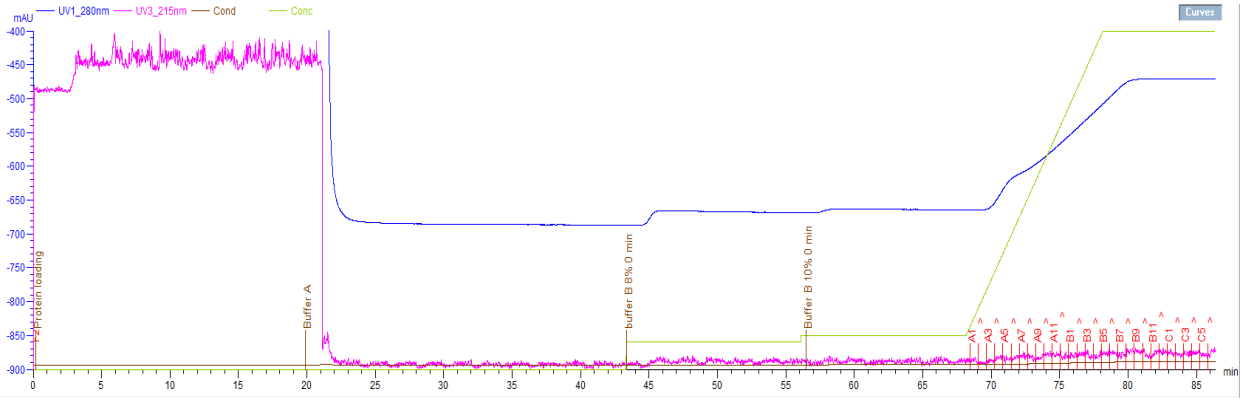

Figure 17. The chromatogram of the SOD1 heterodimer wt-G41D. This figure displays the entire chromatographic process with the equilibration phase using the equilibration buffer containing 40 mM imidazole and 10% elution buffer. For elution, a gradient was applied, increasing to 100% elution buffer over a period of 10 minutes for targeted protein detachment.

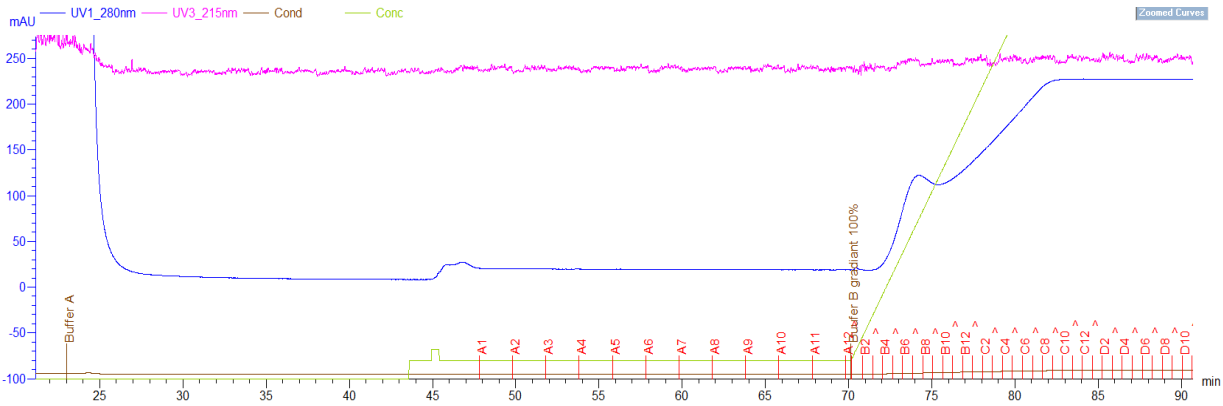

Figure 18. The chromatogram of the SOD1 heterodimer wt-G93A. This figure illustrates the chromatography, including equilibration with an equilibration buffer containing 25 mM imidazole and 5% elution buffer, followed by a 10-minute elution gradient up to 100%.

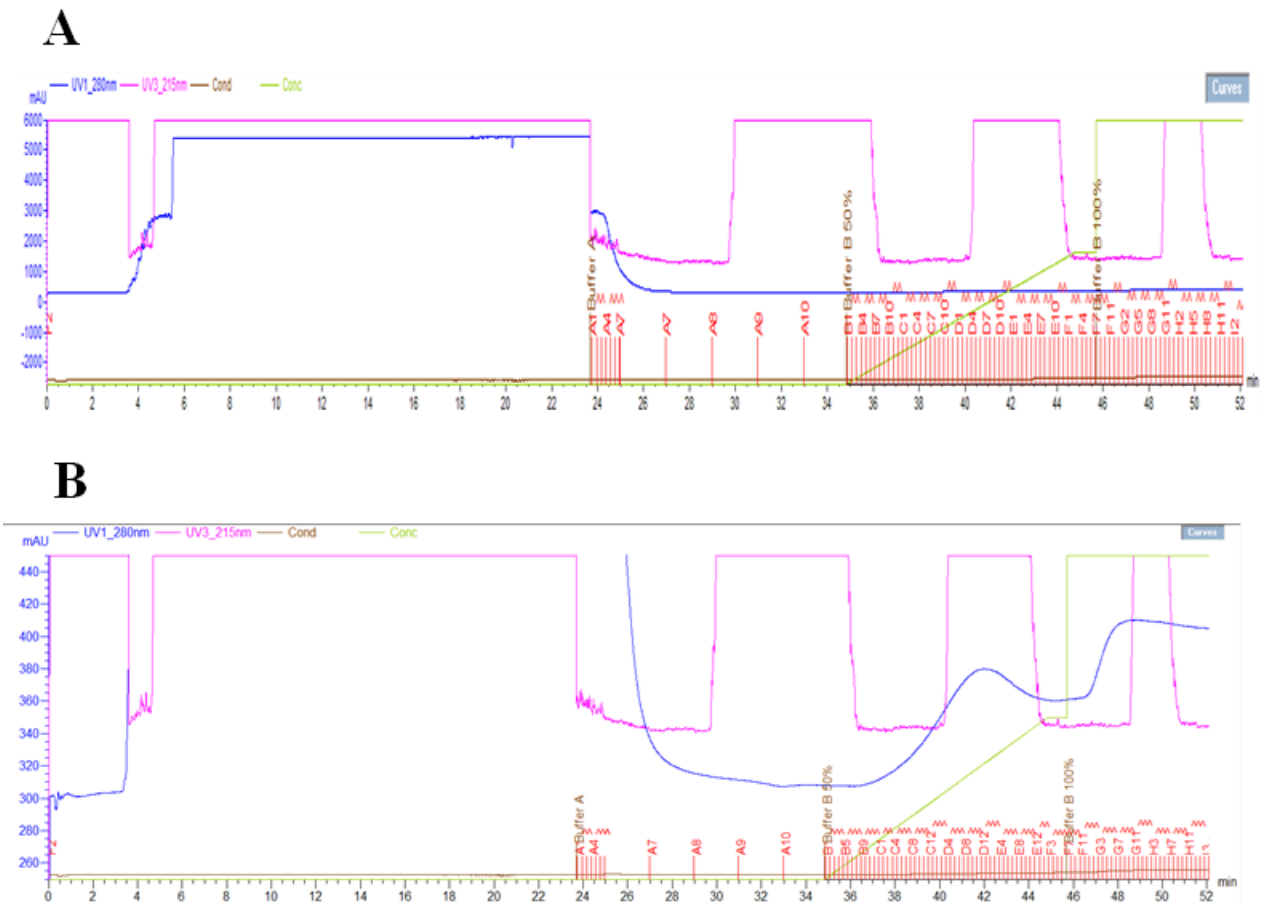

Figure 19. The chromatogram of the SOD1 heterodimer wt-D76V Part A) displays the full chromatography sequence. Part B) zooms in on the equilibration phase using equilibration buffer containing 25 mM imidazole, succeeded by a two-step elution process: initially, a 10-minute gradient reaching 50%, followed by another 10-minute gradient culminating at 100%, with the scale optimized for clarity of intricate details.

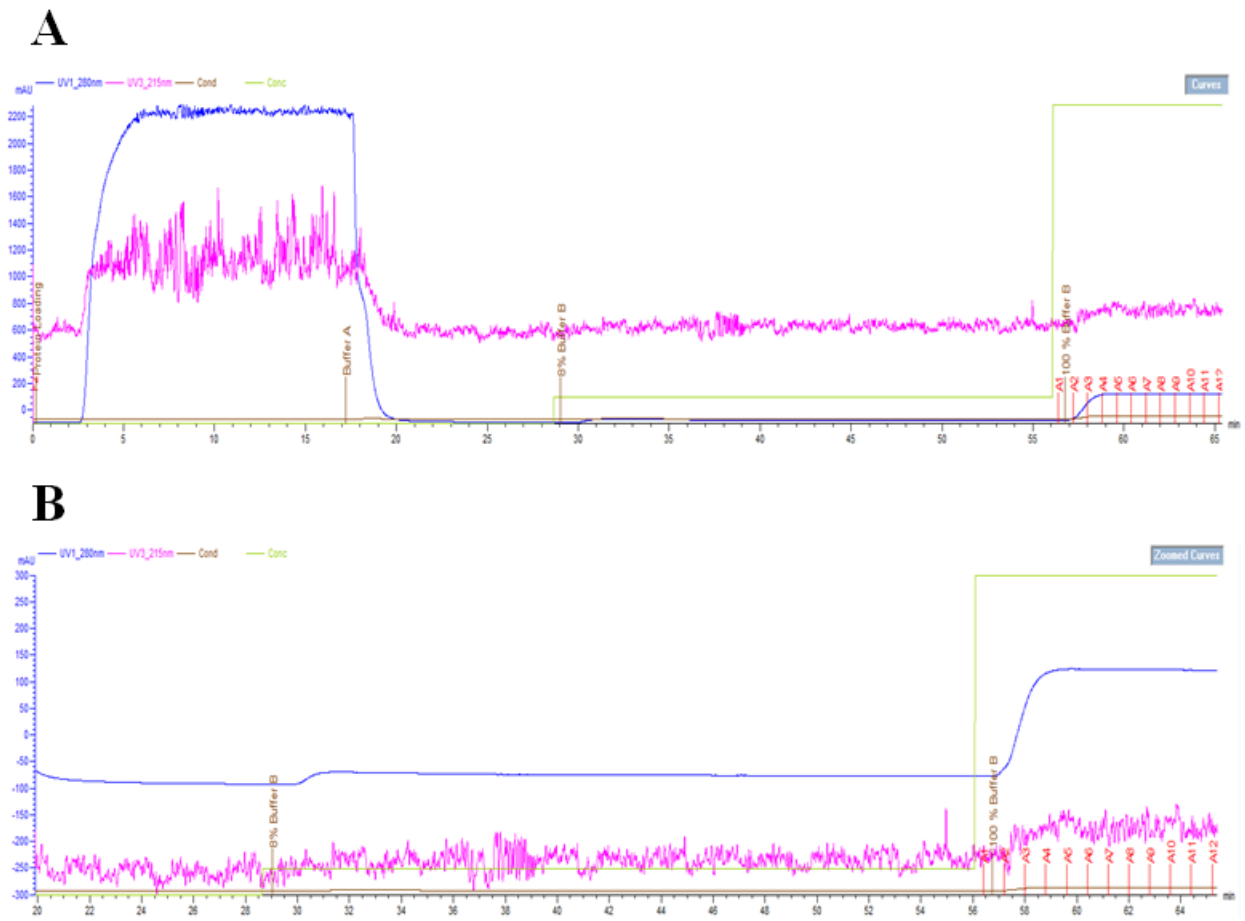

Figure 20. The chromatogram of the SOD1 heterodimer wt-G127X. Part A) illustrates the complete chromatographic process. Part B) focuses on the equilibration stage using an equilibration buffer containing 40 mM imidazole buffer and 8% elution buffer, followed by the elution stage featuring an immediate shift to 100% elution buffer.

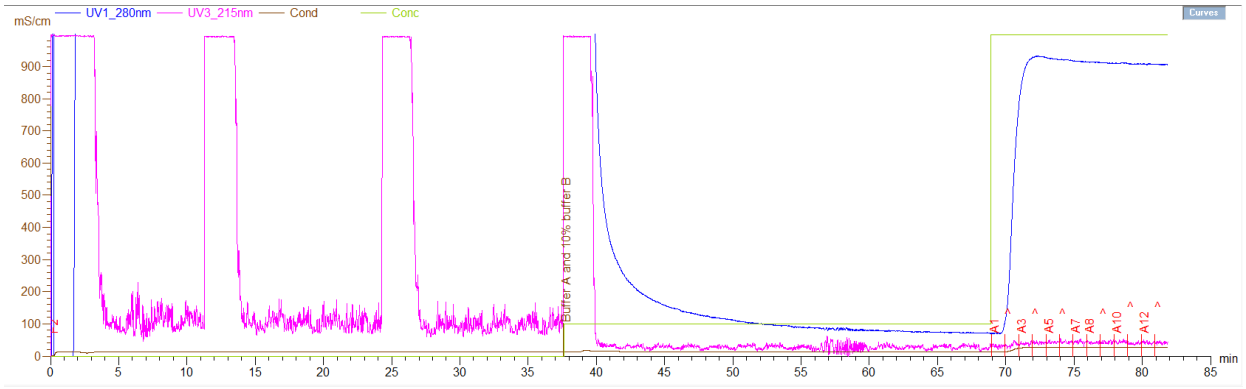

Figure 21. The chromatogram of the SOD1 heterodimer wt-G85R. This figure illustrates the chromatographic sequence, which includes equilibration using a 40 mM imidazole and 10% elution buffer, followed by a rapidly transitioning to a full-strength 100% elution buffer.

The SDS-PAGE analysis of the wt-G41S, wt-G93A, wt-A4V, wt-I104F, wt-G127X, wt-G85R, wt-D76V, and wt-G41D (Figure 22, Figure 23) revealed distinct bands consistent with the purified protein. Notably, bands closer to the bottom of the gel were identified as the tracking dye, which is commonly used to monitor the progression of electrophoresis and does not indicate contamination. Vertical inspection of each lane highlighted a pair of closely situated bands, suggesting the presence of minimal impurities. This observation persisted across purification trials despite alterations to the imidazole concentration in both the equilibration buffer and the purification stages, indicating that the contaminant was not effectively removed under the conditions tested. While this impurity persistence was generally observed, some mutants, such as wt-D76V, wt-G127X, wt-G85R, and wt-G41D, showed very few impurities compared to the rest of purified mutants.

Examining the gel horizontally, four lanes displayed protein elution fractions of varying concentrations. The band intensity diminished from left to right, indicating a reduction in protein concentration in successive fractions. This gradation suggests that the protein eluted in a concentration-dependent manner, with the most concentrated proteins eluting first.

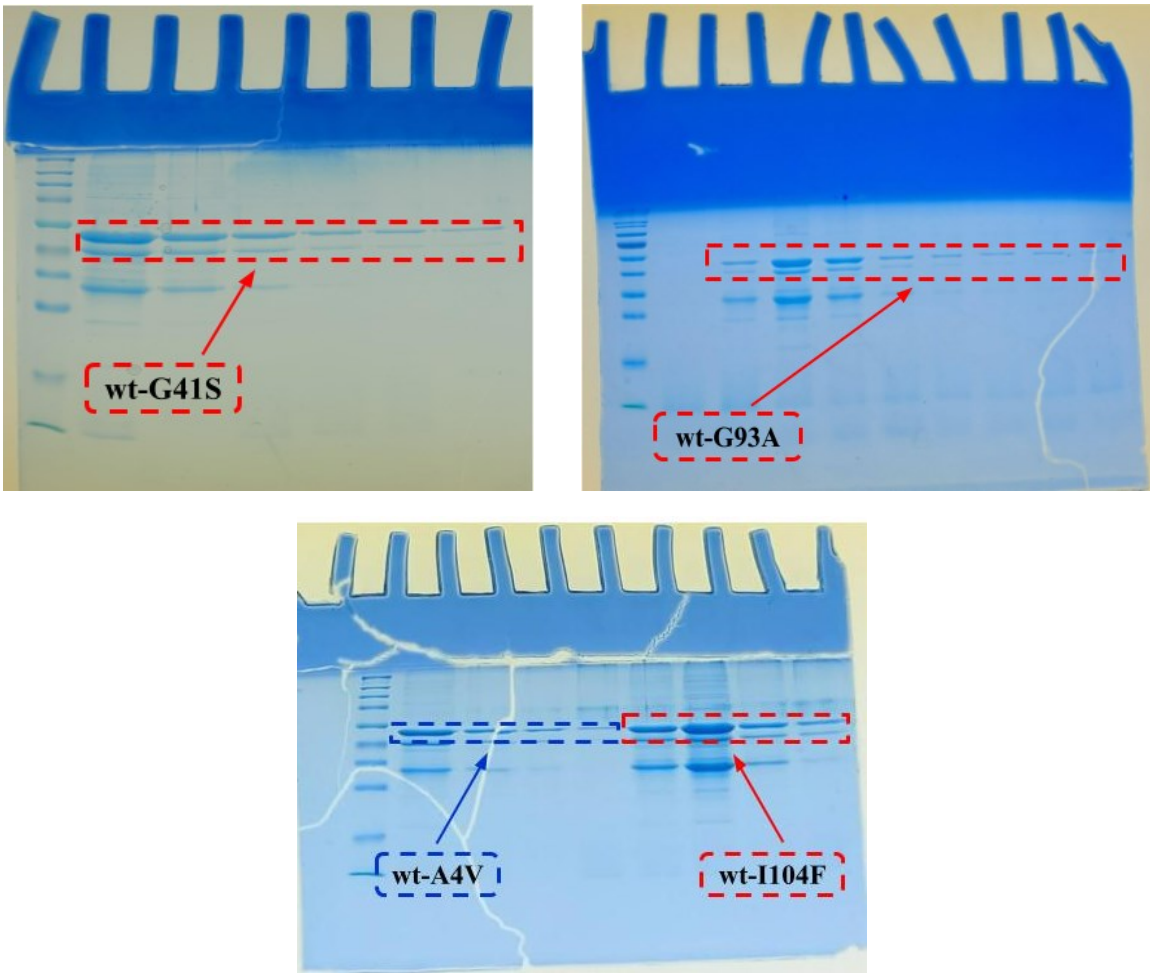

Figure 22. SDS-PAGE of purified wt-G41S, wt-G93A, wt-A4V, and wt-I104F heterodimers. Bands located beneath these borders indicate the presence of impurities within the protein samples. These three heterodimers exhibited more noticeable impurities.

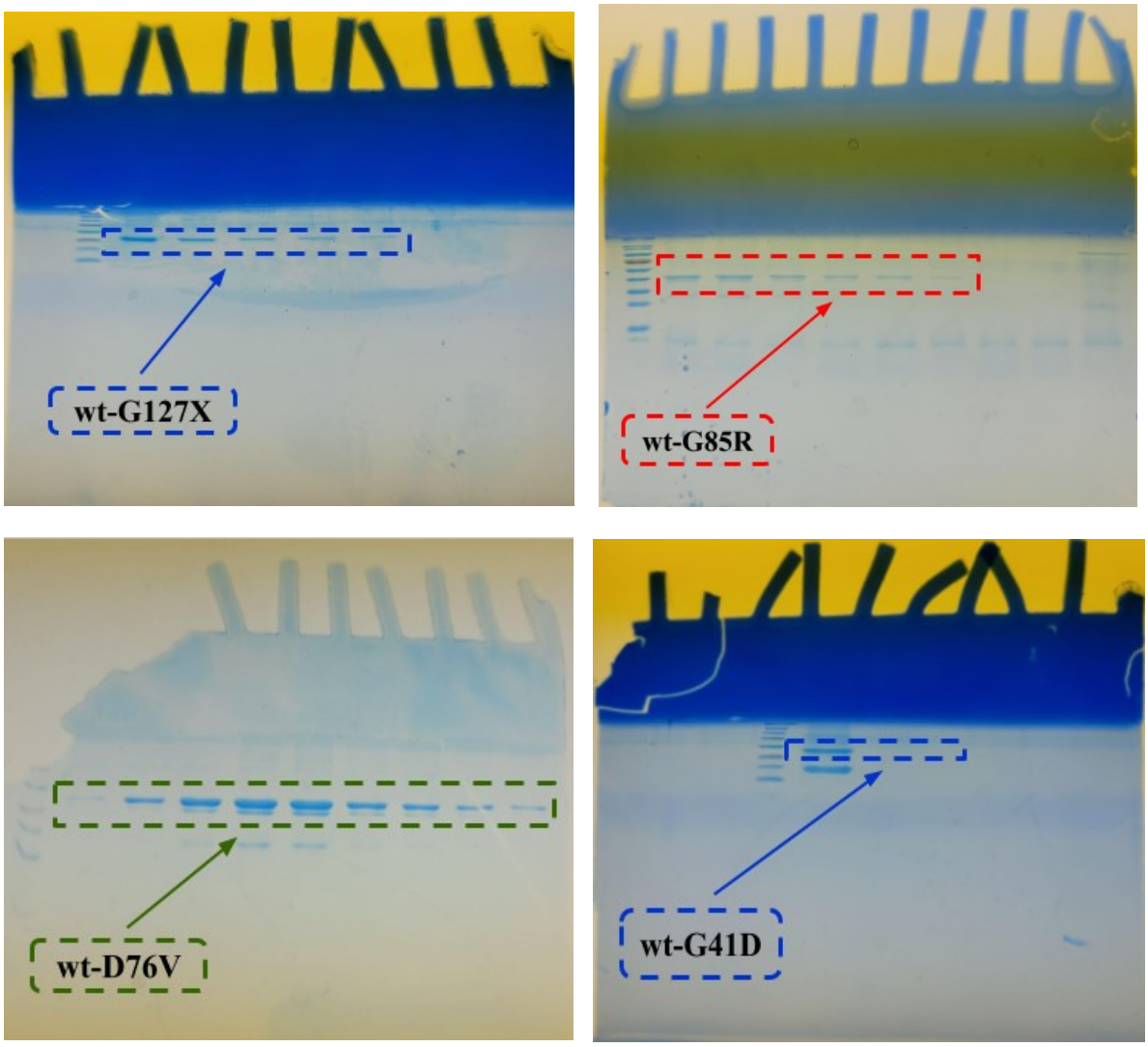

Figure 23. SDS-PAGE of purified wt-G127X, wt-G85R, wt-D76V, and wt-G85R heterodimers. showing. These four heterodimers exhibited very few impurities.

4.2 Prion-like Conversion Results

To assess SOD1 prion-like conversion, the enzymatic activity of the SOD1 heterodimer was monitored, looking for any activity decrease indicative of the wild-type monomer conversion to a misfolded form exhibiting lower activity. The measurement of the activity is based on the heterodimer construct's ability to inhibit peroxide anion reduction; therefore, less inhibition generally suggests more conversion of wt SOD1 to a misfolded form.

Grad et al. have shown that in human neural cells, the expression of the G85R and G127X SOD1 mutants induces misfolding in wt SOD1, indicating the capability of these two mutants to propagate misfolding [91]. Therefore, we performed our first experiments on wt-G85R and wt-G127X heterodimers, as the results were expected, meaning observing no conversion would have been surprising. This approach also provided a reliable baseline to validate the efficacy of our designed assay. Additionally, we performed an experiment with wt-wt homodimers as a control, operating under the presumption that their enzymatic activity would remain stable, given both components are natively folded; thereby, any induction or propagation of misfolding should not be observed.

As illustrated in Figure 24, the inhibition of peroxide anion reduction by wt-wt, wt-G12X and wt-G85R was monitored over 40 hours. The enzymatic activity of the wt-wt homodimer remained stable at approximately 75%, indicating consistent inhibitory performance throughout the experiment. Conversely, wt-G127X and wt-G85R heterodimers demonstrated a decrease in their inhibitory function by approximately 30% and 35%, respectively. During the first hours, they both exhibited a phase of stability in their activity, known as the lag phase, followed by a gradual decline during the conversion phase. This reduction continued until reaching a phase of stability

beyond which their reduced activity plateaued. The observed behavior of wt-G85R and wt-G127X suggests that a sigmoidal curve would be a suitable fit.

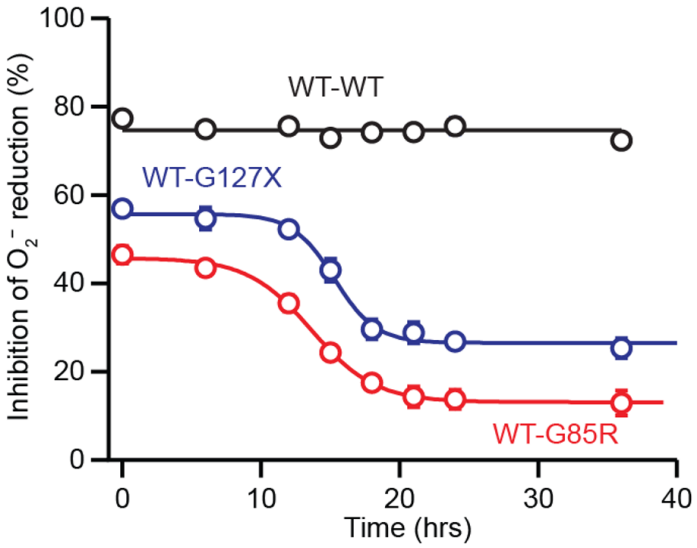

Figure 24. The enzymatic inhibition of O_2^- reduction by wt-wt, wt-G127X and wt-G85R. This graph highlights the differential stability and activity of the SOD1 homodimer and heterodimers. This graph is credited to the work of Abhishek Narayan.

The next round of experiments, aimed to expand our initial study, involved testing on wt-D76V, wt-G93A, wt-G41D, wt-A4V, wt-G41S, and wt-I104F heterodimers to investigate whether wt SOD1 undergo conversion. These specific mutants were selected because each exhibited a specific survival time in ALS cases different from the other, which makes it a broad range of survival times. Also, these mutations are located at different sites within the SOD1 structure. This diversity allows us to investigate if there is a relation between mutation sites within the SOD1 protein and the rate of propagation of misfolding and the progression of ALS pathology.

Three of these heterodimers, wt-D76V, wt-G93A, and wt-G41D, showed a drop in activity after a lag phase with a sigmoidal pattern (Figure 25) similar to what was previously seen in wt-G85R and wt-G127X activity. Two other heterodimers, wt-A4V and wt-G41S, maintained stable activity levels throughout the experiment, exhibiting no obvious changes in their activity (Figure 26), and finally, wt-I104F demonstrated a decrease in activity in a more complex pattern than other heterodimers (Figure 27).

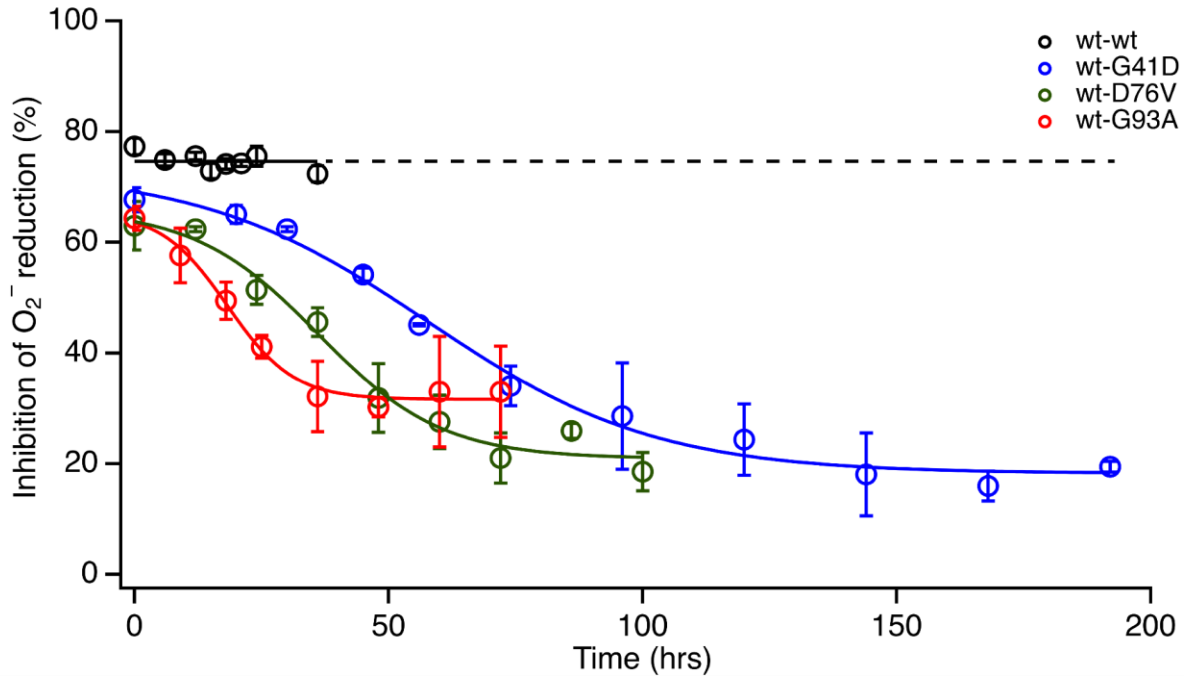

Figure 25. The enzymatic inhibition of O_2^- reduction by wt-wt, wt-G41D, wt-D76V, and wt-G93A. The activity of these three heterodimers exhibits a gradual decline after an initial lag phase, following a sigmoidal pattern similar to what is observed for wt-G85R and wt-G127X activities. Error bars represent the standard error of the mean calculated from three replicates.

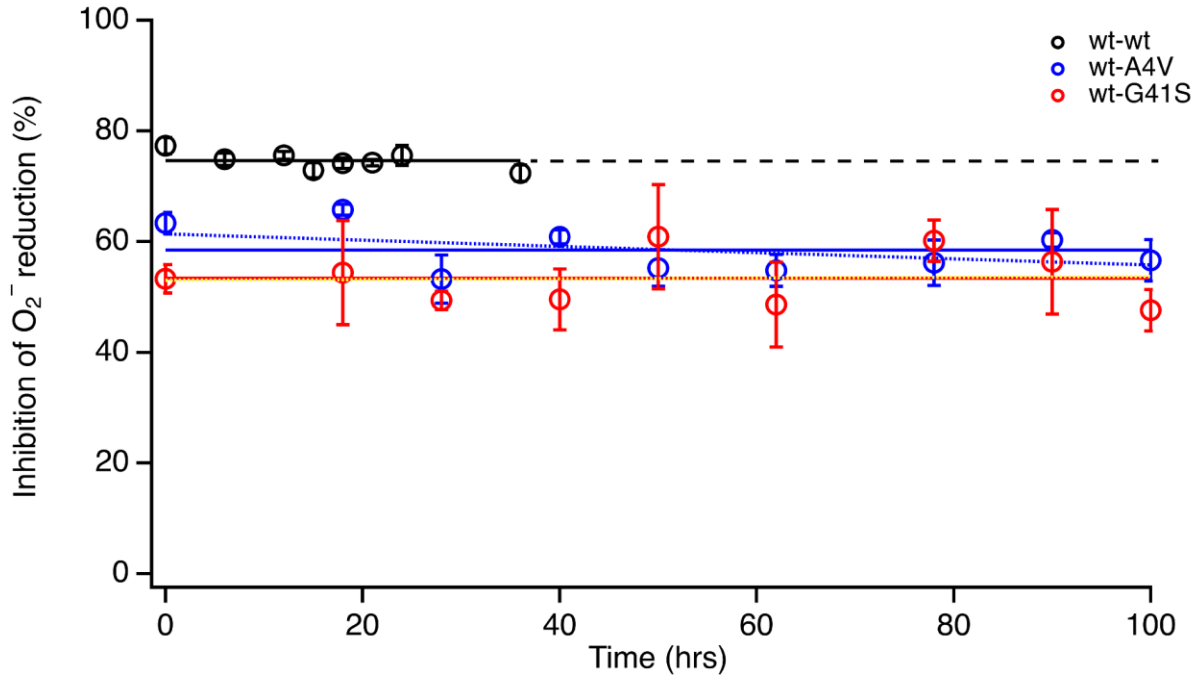

Figure 26. The enzymatic inhibition of O_2^- reduction by wt-wt, wt-A4V, and wt-G41S. The activity of the two heterodimers remains stable without notable change over the observed period. The primary fit, indicated by dotted lines, aligns with a zero slope, leading to the application of a secondary straight-line fit with a slope of zero. Error bars represent the standard error of the mean calculated from three replicates.

The observed pattern in the enzyme activities of wt-G41D, wt-D76V, and wt-G93A was similar to what we observed for wt-G85R and wt-G127X, suggesting that a sigmoidal curve, based on the same equation used for wt-G127X and wt-G85R, would be an appropriate fitting curve for describing these three heterodimers enzymatic activity and quantifying the conversions. The parameters derived from these sigmoidal curves (Table 1) provide a basis for a comparative analysis highlighting each mutation's distinct effects on the prion-like conversion of wt SOD1.

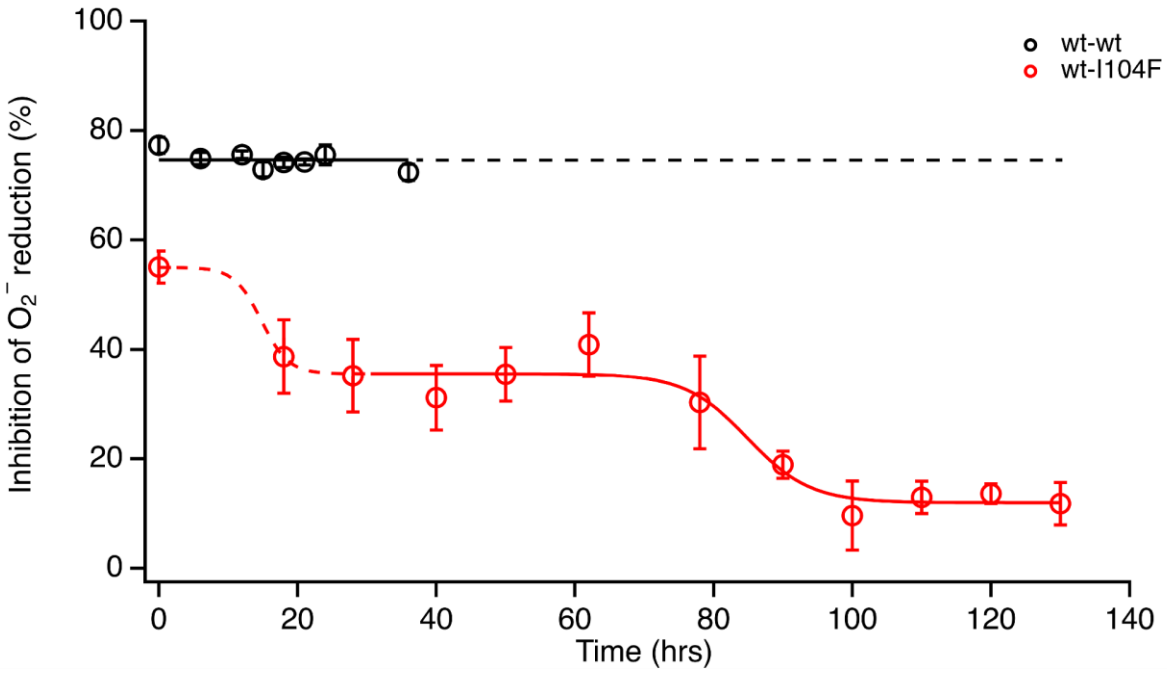

Figure 27. The enzymatic inhibition of O_2^- reduction by wt-I104F. The activity of this heterodimer shows a decline in two distinct phases. The dashed line in the wt-104F graph represents a tentative sigmoidal fit, as the rapid changes and lack of enough data points in the initial phase make it hard to describe the observed pattern precisely with a certain fitting model. Error bars denote the standard error of the mean calculated from three replicates.

Looking at the initial percentage inhibition of the superoxide anion reduction, all heterodimers started at a lower level than the wt-wt homodimer. Between heterodimers, wt-G85R started at the lowest value compared to the others, while wt-G41D began with the highest initial inhibition and was closest to the initial inhibition value of wt-wt.

Regarding the maximal change in inhibition from baseline, noticeably, wt-G41D showed the greatest reduction with a 55 ± 5% decrease in activity from the start point, indicating a more substantial alteration in activity. On the other hand, wt-G127X, wt-G85R, and wt-G93A demonstrated the least amount of decrease in activity with 29 ± 1%, 33 ± 1%, and 34 ± 3% reduction from the initial activity, respectively.

The parameter $t_{1/2}$ represents the time it takes for the inhibition of the superoxide anion reduction to reduce by half, or in other words, the enzymatic activity of a heterodimer reaches half of its initial amount. While some heterodimers like wt-G85R and wt-G127X have relatively shorter $t_{1/2}$ values within a close range, wt-D76V and wt-G41D showed markedly longer $t_{1/2}$, even when accounting for fitting errors. This suggests that the conversion process in wt-D76V and wt-G41D is significantly slower in time.

Regarding the transition rate during the conversion phase, which relates to the steepness of the sigmoidal curve once the decrease started, wt-G41D exhibited a more gradual transition indicated by a larger τ value, suggesting a slower rate of inhibition decrease. Conversely, wt-G85R and wt-G127X displayed a sharper transition with smaller τ values, indicating a faster rate of inhibition decrease. These differences are significant even when considering the variability indicated by the error margins of the fits.

SOD1 heterodimers	Initial value of inhibition (%)	Maximal change from baseline (%)	$t_{1/2}$ (hrs)	τ (hrs)
wt-G85R	45.7 ± 0.7	33 ± 1	13.6 ± 0.2	2.3 ± 0.2
wt-G127X	56 ± 1	29 ± 1	15.3 ± 0.3	1.5 ± 0.3
wt-D76V	66 ± 5	45 ± 6	36 ± 4	12 ± 4
wt-G93A	66 ± 3	34 ± 3	18 ± 2	7 ± 2
wt-G41D	73 ± 4	55 ± 5	58 ± 4	22 ± 4

Table 3. Sigmoidal fit parameters for wt-G85R, wt-G127X, wt-D76V, wt-G93A, and wt-G41D heterodimers

SOD1 heterodimers wt-A4V and wt-G41S demonstrated a lower mean value of percentage inhibition of superoxide anion reduction compared to the wt-wt homodimer. A linear fit was applied given the lack of significant change and maintained stability in their activity. The resulting slopes of -0.06 ± 0.04 for wt-A4V and 0.01 ± 0.06 for wt-G41S are consistent with a negligible slope, verifying the use of a final straight-line fit with a zero slope.

SOD1 heterodimers	Mean value of Inhibition (%)	Rate (%/hrs)
wt-wt	74.6 ± 0.6	-0.10 ± 0.04
wt-A4V	58 ± 1	-0.06 ± 0.04
wt-G41S	53 ± 2	0.01 ± 0.06

Table 4. Straight-line fit parameters for wt-wt homodimer and wt-A4V and wt-G41S heterodimers

The enzymatic activity of wt-I104F, starting with an initial percentage inhibition of superoxide anion reduction at 55 ± 5%, exhibited a biphasic decrease pattern. A rapid decline was observed initially, plateauing shortly after, followed by a much slower decline before stabilizing. The initial decline in activity suggests a potential single-phase transition within the first 5 to 15 hours. The rapid changes in the initial phase make it hard to describe the observed pattern precisely with a certain fitting model. Also, there are not enough data points to quantify the kinetics of the first transition accurately.

The second phase showed a much more gradual decrease, aligned with a sigmoidal curve. Notably, the maximal decrease in activity was roughly similar for both phases: 19 ± 6% initially, followed by 24 ± 3% in the latter phase. Further research is required to characterize the initial phase of wt-I104F activity more accurately. It is a provisional assumption that the initial transition may follow a sigmoidal pattern.

4.3 Discussion

This study is the first to systematically investigate which SOD1 mutants associated with familial ALS can induce prion-like propagation of misfolding, as well as the timeline and rate of such transformations. It specifically quantifies the prion-like conversion of wt SOD1 by different SOD1 mutants to address the mentioned aspects of prion-like conversion, underscoring the novelty and significance of this research.

The SOD1 homodimer wt-wt exhibited consistent enzymatic activity throughout the assay, indicating that wt-wt interactions do not lead to misfolding under the experiment. This observation serves as a critical control, establishing a baseline for comparison with other SOD1 heterodimers' enzymatic activity. The lower initial activity level of SOD1 heterodimers, compared to the wt-wt suggests that specific mutations may affect protein structure and function. However, these observed differences might also arise from something more subtle, such as lower affinity of SOD1 mutant for the copper or challenges in copper ion insertion by chaperones.

SOD1 heterodimers wt-G85R, wt-G127X, wt-G41D, wt-D76V, and wt-G93A exhibited a sigmoidal decline in enzymatic activity. This pattern aligns with the prion-like conversion mechanism, where a decline follows an initial phase of stability in function as more native proteins undergo misfolding. The final phase of stability suggests a saturation point where most native structures have been converted. This sigmoidal pattern is like what is seen for protein aggregation,

where a slow nucleation process leads to a lag phase, followed by rapid growth and saturation when all the proteins are aggregated [111], [112]. However, a study on SOD1 heterodimers wt-G85R and wt-G127X using mass photometry shows that the decrease in the activity is not related to the protein aggregation, suggesting that the activity reduction is due to prion-like conversion in individual heterodimers [100].

In this case, the most straightforward model to describe the conversion would be a single-exponential decay, which typically does not include a lag phase [113]. However, the presence of a lag phase in the observed prion-like conversion patterns suggests that the conversion process involves multiple steps. As a result, the time distribution for a given molecule to undergo conversion does not remain constant; instead, it tends to peak at a value greater than zero. This phenomenon occurs due to the convolution of several single-exponential distributions, each representing different steps in the conversion process, which collectively contribute to the emergence of a lag phase. The size of this lag phase and the steepness of the subsequent activity decline may be related to the rates of various microscopic steps involved in the SOD1 conversion process. However, distinguishing these rates can be complex due to their convolution.

Upon conversion, the heterodimers that displayed a sigmoidal pattern for conversion showed varying amplitudes in their activity changes. This variation suggests that the efficiency of conversion, which refers to the proportion of wild-type SOD1 molecules that undergo conversion, might differ among the mutants. Alternatively, it is possible that the activity level of the wild-type domain within the converted state varies across different mutants. This could be due to each mutant potentially templating distinct misfolded structures, each with its own unique activity profile. However, distinguishing between these possibilities remains a challenge in our study.

The SOD1 heterodimers wt-A4V and wt-G41S demonstrated notable stability, with their enzymatic activity remaining largely unchanged. This observation in the prion-like conversion pattern could be attributed to the possibility that the mutants retain some activity of their own. If a mutant is misfolded but continues to exhibit activity levels comparable to the wild-type, then a conversion of the wild-type domain may not lead to any detectable change in activity. Consequently, the conversion pattern would exhibit no significant alterations. Additionally, it is plausible that the conversion rate of these mutants is slower, potentially becoming apparent only over an extended observation period. The other possibility is that these mutants are not able to convert wt domain; therefore, no activity change is shown.

The wt-I104F heterodimer exhibited a biphasic reduction in enzymatic activity, distinct from the patterns observed in other heterodimers. This suggests that the mutant may undergo two separate processes. One explanation for the biphasic activity decline is that initially, the mutant is not in a misfolded state; therefore, it has native-like activity levels. The initial phase could involve a misfolding process, potentially induced by the mildly denaturing and reducing conditions used to promote conversion in the assay. Following this misfolding, the mutant can convert the wt domain into the misfolded state, accounting for the second distinct phase observed in the activity data.

One point that should be kept in mind is that before publication, we would want to repeat the measurements with controls (wt-wt) continued for the whole period of the conversion process to ensure that the observations are robust and to rule out any potential variability in the assay conditions or temporal stability of the enzyme.

In this study, one of the interesting questions we explored was whether the rapidity with which fALS progresses in patients correlates with the lag time observed for wt SOD1 conversion by different mutants. Initially, we hypothesized that there might be a relation between the time it

takes for wt SOD1 to be converted by a specific mutant and the survival time of that mutant's associated ALS, meaning the faster the conversion process, the faster the disease spreads, hence the shorter survival time. Figure 28 illustrates the data of patients' survival times and $t_{1/2}$ obtained from the activity graphs of explored SOD1 heterodimers, which helps to test this hypothesis. Despite not showing any noticeable change in activity, AV4 and G41S were also included on this graph, represented as distinct points due to their undefined $t_{1/2}$. The graph shows no obvious correlation between survival time and conversion time; hence, the initial hypothesis is rejected.

The fact that why some SOD1 mutations lead to very aggressive disease, whereas some have significantly extended survival times, remains unclear in ALS research. Previous investigations into SOD1 mutants have not found strong links between specific mutant properties and disease severity [34], [114], [115], [116], [117], [118], [119]. Given that conversion time has not been studied in this context, it was assumed that this factor might hold significance. However, the data obtained so far (from a limited number of mutants) do not support a direct relationship.

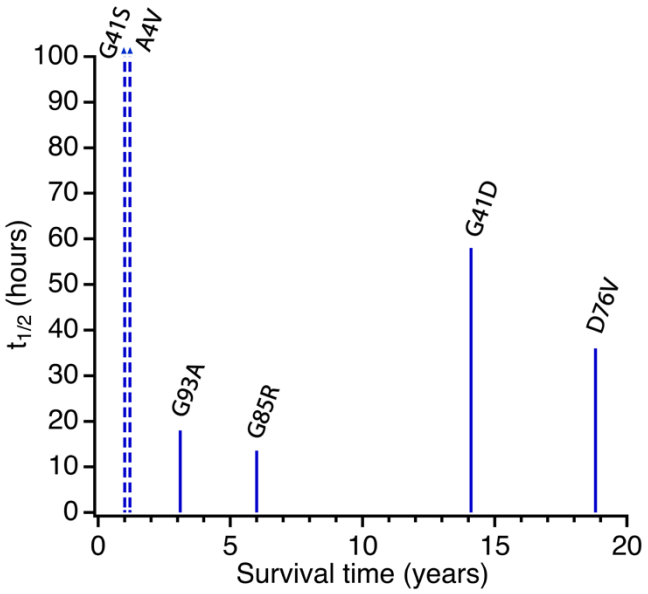

Figure 28. Correlation between SOD1 mutants' conversion times and ALS patient survival times. This graph assesses the relationship between the half-life of SOD1 mutant conversions and the survival times of ALS patients carrying these mutations. The data reveals an absence of a clear and direct correlation. wt-G41D and Mutants wt-G41S and wt-A4V maintain consistent enzymatic activity, making their $t_{1/2}$ immeasurable, represented here by a dashed line extending towards infinity. Survival time data for ALS patients with specific SOD1 mutations are adapted from [34], [115], [116], [117], [118]

This research has shed light on the diverse prion-like conversion abilities of various fALS-associated SOD1 mutations. While we have advanced our knowledge of how different mutations affect protein misfolding propagation, the connection between these conversion processes and ALS's actual progression remains unclear. The findings suggest that despite the lack of a clear connection, the role of prion-like conversion in the pathogenesis of the disease is an important area for future investigation. Further studies are essential to discover which aspects of these mutants contribute to the different ALS outcomes and severity. Even though we could not find a meaningful relation between prion-like conversion of wt SOD1 by different mutants and the severity of ALS,

our findings are nonetheless significant. They highlight the complexity of the disease and the necessity for continued research to unravel the relationship between prion-like conversion and ALS pathology.

Chapter 5: Conclusions and Future Work

This study focused on the prion-like conversion of natively folded wild-type SOD1, a protein linked to ALS, by various SOD1 mutants. Inspired by the prion interactions seen in prion diseases, we investigated how misfolded SOD1 interacts with and induces misfolding in wild-type SOD1, leading to the propagation of this misfolded structure. Our experiments were conducted using heterodimer structures comprising a wild-type SOD1 monomer tethered to a mutant SOD1 monomer with a 50 amino acid-long tether. To monitor prion-like propagation, we designed an assay tracking the enzymatic activity of wt SOD1, considering the decrease in enzymatic activity as a potential marker of conversion. We performed our experiments on the wt-wt homodimer as control and wt-G85R, wt-G127X, wt-D76V, wt-G93A, wt-G41D, wt-I104F, wt-G41S, and wt-A4V heterodimers.

Our findings revealed a sigmoidal decline in the enzymatic activity of certain heterodimers, such as wt-G85R, wt-G127X, wt-G41D, wt-D76V, and wt-G93A. Initially, these heterodimers showed a stable phase of activity, followed by a decrease representing the conversion phase, and finally reaching stability, suggesting the completion of the conversion. This pattern indicated that a sigmoidal curve would be an appropriate fit for the observed data.

The wt-A4V and wt-G41S heterodimers maintained stable enzymatic activity throughout the experiment, suggesting that these mutants either retain some functional activity when misfolded or have a slower conversion rate. The wt-I104F heterodimer demonstrated a biphasic pattern in its activity decline, distinct from the other mutants, indicating a possible two-step conversion process.

The pattern seen in the enzymatic activity of tested heterodimers assisted in quantifying the prion-like conversion, which provides insights into the timeline and rate of such conversions.

Between heterodimers, the wt-G41D heterodimer showed the highest maximal change in activity and presented a more gradual transition phase, implying that the conversion extended over a longer duration. Also, it took the longest to reach half of its initial activity. In contrast, wt-G85R and wt-G127X displayed relatively quick transition phases, resulting in steeper conversion curves coupled with shorter times to half-maximal activity or, in other words, smaller $t_{1/2}$, suggesting a more rapid conversion process.

Our investigation into the correlation between the rapidity of fALS progression in patients and the lag time observed for wt SOD1 conversion by different mutants revealed no direct relation, challenging our initial hypothesis that a faster conversion equates to more aggressive disease progression and a shorter survival time.

This study motivates us to conduct further studies to explore various aspects of prion-like conversion and propagation of misfolded SOD1 structure. One key area involves developing a microscopic model to accurately describe the prion-like conversion process, particularly for heterodimers exhibiting a lag phase and a sigmoidal decline in activity. This model would consider the convolution of various single-exponential distributions representing the different stages of conversion [113]. By analyzing the lag phase and activity decline rates, we can gain insights into the microscopic steps involved in the conversion process.

A future area of work involves conducting additional experiments on wt-I104F to collect more data points, especially for the first phase, so that we can define a more accurate pattern for the conversion of this heterodimer. Then, we could fit the data on the mentioned microscopic model to assess and validate the model's accuracy in describing the conversion process.
Additionally, expanding our research to investigate a wider range of the over 220 known SOD1 mutants could potentially uncover a meaningful correlation between the rapidity of ALS

progression and conversion time, a connection that may have remained undetected in our current research due to the limited number of mutants that has been looked into.

Building on recent findings, introducing proline mutations into specific regions of a SOD1 protein mutant significantly reduces aggregation and toxicity [36]. Further exploration of these mutations with our assay could be invaluable. Assessing how these specific proline substitutions affect the prion-like conversion of SOD1 can offer deeper insights into the critical regions and mechanisms of SOD1 prion-like conversion.

Another promising direction is extending conversion studies using Förster Resonance Energy Transfer (FRET). This method directly observes structural changes during the conversion process, providing a valuable alternative perspective to enzymatic activity assays.

With these future directions, we aim to unravel the complexities of SOD1 prion-like conversion further, advancing our understanding of ALS and paving the way for new possibilities in therapeutic interventions.

References

[1] C. Soto and S. Pritzkow, “Protein misfolding, aggregation, and conformational strains in neurodegenerative diseases,” *Nat Neurosci*, vol. 21, no. 10, pp. 1332–1340, Oct. 2018, doi: 10.1038/s41593-018-0235-9.

[2] S. B. Prusiner, “Prions,” *Proc Natl Acad Sci U S A*, vol. 95, no. 23, pp. 13363–13383, Nov. 1998, doi: 10.1073/PNAS.95.23.13363.

[3] J. Hardy and D. J. Selkoe, “The Amyloid Hypothesis of Alzheimer’s Disease: Progress and Problems on the Road to Therapeutics,” *Science (1979)*, vol. 297, no. 5580, pp. 353–356, 2002, [Online]. Available: http://science.sciencemag.org/

[4] K. Iqbal, F. Liu, C.-X. Gong, and I. Grundke-Iqbal, “Tau in Alzheimer Disease and Related Tauopathies,” *Curr Alzheimer Res*, vol. 7, no. 8, pp. 656–664, Dec. 2010, doi: 10.2174/156720510793611592.

[5] M. Goedert, M. G. Spillantini, K. Del Tredici, and H. Braak, “100 years of Lewy pathology,” *Nat Rev Neurol*, vol. 9, no. 1, pp. 13–24, Jan. 2013, doi: 10.1038/nrneurol.2012.242.

[6] F. Akçimen *et al.*, “Amyotrophic lateral sclerosis: translating genetic discoveries into therapies,” *Nat Rev Genet*, vol. 24, no. 9, pp. 642–658, Sep. 2023, doi: 10.1038/s41576-023-00592-y.

[7] C. A. Ross and M. A. Poirier, “Protein aggregation and neurodegenerative disease,” *Nat Med*, vol. 10, no. 7, p. S10, 2004, doi: 10.1038/nm1066.

[8] K. A. Jellinger, “Basic mechanisms of neurodegeneration: A critical update,” *J Cell Mol Med*, vol. 14, no. 3, pp. 457–487, Mar. 2010, doi: 10.1111/j.1582-4934.2010.01010.x.

[9] K. A. Jellinger, “Recent advances in our understanding of neurodegeneration,” *J Neural Transm*, vol. 116, no. 9, pp. 1111–1162, Sep. 2009, doi: 10.1007/s00702-009-0240-y.

[10] D. M. Skovronsky, V. M. Y. Lee, and J. Q. Trojanowski, “Neurodegenerative diseases: New concepts of pathogenesis and their therapeutic implications,” *Annu Rev Pathol*, vol. 1, pp. 151–170, 2006, doi: 10.1146/annurev.pathol.1.110304.100113.

[11] L. C. Walker and M. Jucker, “Neurodegenerative Diseases: Expanding the Prion Concept,” *Annu Rev Neurosci*, vol. 38, pp. 87–103, Jul. 2015, doi: 10.1146/annurev-neuro-071714-033828.

[12] F. Chiti and C. M. Dobson, “Protein misfolding, functional amyloid, and human disease,” *Annu Rev Biochem*, vol. 75, pp. 333–366, 2006, doi: 10.1146/annurev.biochem.75.101304.123901.

[13] N. R. Cashman and B. Caughey, “Prion diseases - Close to effective therapy?,” *Nat Rev Drug Discov*, vol. 3, no. 10, pp. 874–884, Oct. 2004, doi: 10.1038/nrd1525.

[14] K. M. Pan *et al.*, “Conversion of alpha-helices into beta-sheets features in the formation of the scrapie prion proteins.,” *Proc Natl Acad Sci U S A*, vol. 90, no. 23, p. 10962, Dec. 1993, doi: 10.1073/PNAS.90.23.10962.

[15] B. Caughey, G. S. Baron, B. Chesebro, and M. Jeffrey, “Getting a grip on prions: Oligomers, amyloids, and pathological membrane interactions,” *Annu Rev Biochem*, vol. 78, pp. 177–204, 2009, doi: 10.1146/annurev.biochem.78.082907.145410.

[16] D. W. Colby and S. B. Prusiner, “Prions,” *Cold Spring Harb Perspect Biol*, vol. 3, no. 1, pp. 1–22, Jan. 2011, doi: 10.1101/cshperspect.a006833.

[17] B. Frost and M. I. Diamond, “Prion-like Mechanisms in Neurodegenerative Diseases,” *Nat Rev Neurosci*, vol. 11, no. 3, pp. 155–159, Mar. 2010, doi: 10.1038/NRN2786.

[18] J. Vaquer-Alicea and M. I. Diamond, “Propagation of Protein Aggregation in Neurodegenerative Diseases,” *Annu Rev Biochem*, vol. 88, pp. 785–810, Jun. 2019, doi: 10.1146/ANNUREV-BIOCHEM-061516-045049.

[19] I. Acquatella Tran Van Ba, T. Imberdis, and V. Perrier, “From prion diseases to prion-like propagation mechanisms of neurodegenerative diseases,” *Int J Cell Biol*, vol. 2013, 2013, doi: 10.1155/2013/975832.

[20] O. Hardiman *et al.*, “Amyotrophic lateral sclerosis,” *Nat Rev Dis Primers*, vol. 3, no. 17071, Oct. 2017, doi: 10.1038/nrdp.2017.71.

[21] National Institute of Neurological Disorders and Stroke (NINDS), “Amyotrophic Lateral Sclerosis (ALS),” National Institute of Neurological Disorders and Stroke (NINDS). Accessed: Jan. 05, 2024. [Online]. Available: https://www.ninds.nih.gov/health-information/disorders/amyotrophic-lateral-sclerosis-als

[22] T. Alfahad and A. Nath, “Retroviruses and amyotrophic lateral sclerosis,” *Antiviral Res*, vol. 99, no. 2, pp. 180–187, 2013, doi: 10.1016/j.antiviral.2013.05.006.

[23] K. C. Arthur, A. Calvo, T. R. Price, J. T. Geiger, A. Chiò, and B. J. Traynor, “Projected increase in amyotrophic lateral sclerosis from 2015 to 2040,” *Nature Communications 2016 7:1*, vol. 7, no. 1, pp. 1–6, Aug. 2016, doi: 10.1038/ncomms12408.

[24] “World Population Ageing 2013,” *United Nations, Department of Economic and Social Affairs, Population Division*, vol. ST/ESA/SER.A/348, 2013.

[25] K. Sen and R. Bonita, “Global health status: Two steps forward, one step back,” *Lancet*, vol. 356, no. 9229, pp. 577–582, Aug. 2000, doi: 10.1016/S0140-6736(00)02590-3.

[26] A. Chiò *et al.*, “Global epidemiology of amyotrophic lateral sclerosis: A systematic review of the published literature,” *Neuroepidemiology*, vol. 41, no. 2, pp. 118–130, Aug. 2013, doi: 10.1159/000351153.

[27] H. Blasco, F. Patin, C. R. Andres, P. Corcia, and P. H. Gordon, “Amyotrophic Lateral Sclerosis, 2016: existing therapies and the ongoing search for neuroprotection,” *Expert Opin Pharmacother*, vol. 17, no. 12, pp. 1669–1682, Aug. 2016, doi: 10.1080/14656566.2016.1202919.

[28] E. (MCI-186) A. 19 S. G. Writing Group, “Safety and efficacy of edaravone in well defined patients with amyotrophic lateral sclerosis: a randomised, double-blind, placebo-controlled trial,” *Lancet Neurol*, vol. 16, pp. 505–512, 2017.

[29] F. Laferrièrea and M. PolymenidouPhD, “Advances and challenges in understanding the multifaceted pathogenesis of amyotrophic lateral sclerosis,” *Swiss Med Wkly*, vol. 145, no. 0506, Jan. 2015, doi: 10.4414/smw.2015.14054.

[30] C. J. Weydert and J. J. Cullen, “Measurement of superoxide dismutase, catalase and glutathione peroxidase in cultured cells and tissue,” *Nat Protoc*, vol. 5, no. 1, pp. 51–66, Jan. 2010, doi: 10.1038/nprot.2009.197.

[31] I. N. Zelko, T. J. Mariani, and R. J. Folz, “Superoxide dismutase multigene family: a comparison of the CuZn-SOD (SOD1), Mn-SOD (SOD2), and EC-SOD (SOD3) gene structures, evolution, and expression,” *Free Radic Biol Med*, vol. 33, no. 3, pp. 337–349, Aug. 2002.

[32] L. Y. Chang, J. W. Slot, H. J. Geuze, and J. D. Crapo, “Molecular immunocytochemistry of the CuZn superoxide dismutase in rat hepatocytes.,” *Journal of Cell Biology*, vol. 107, no. 6, pp. 2169–2179, Dec. 1988, doi: 10.1083/JCB.107.6.2169.

[33] D. W. Colby and S. B. Prusiner, “Prions,” *Cold Spring Harb Perspect Biol*, vol. 3, no. 1, pp. 1–22, Jan. 2011, doi: 10.1101/cshperspect.a006833.

[34] D. R. Rosen *et al.*, “Mutations in Cu/Zn superoxide dismutase gene are associated with familial amyotrophic lateral sclerosis,” *Nature*, vol. 362, no. 6415, pp. 59–62, 1993.

[35] G.-A. Keller, T. G. Warner, K. S. Steimert, and R. A. Hallewellt, “Cu,Zn superoxide dismutase is a peroxisomal enzyme in human fibroblasts and hepatoma cells,” *Proc. Nati. Acad. Sci. USA*, vol. 88, no. 16, pp. 7381–7385, 1991.

[36] L. Mcalary, J. R. Nan, C. Shyu, S. S. Plotkin, N. R. Cashman, and N. Cashman, “Amyloidogenic regions in beta-strands II and III modulate the aggregation and toxicity of SOD1 in living cells,” *bioRxiv*, p. 2023.10.18.562627, Oct. 2023, doi: 10.1101/2023.10.18.562627.

[37] J. Huai and Z. Zhang, “Structural properties and interaction partners of familial ALS-associated SOD1 mutants,” *Front Neurol*, vol. 10, no. MAY, p. 456273, May 2019, doi: 10.3389/FNEUR.2019.00527/BIBTEX.

[38] “SOD1,” Wikipedia. Accessed: Jan. 05, 2024. [Online]. Available: https://en.wikipedia.org/wiki/SOD1

[39] D. P. Clark, N. J. Pazdernik, and M. R. McGehee, “Protein Synthesis,” *Mol Biol*, pp. 397–444, 2019.

[40] C. M. Dobson, “Protein folding and misfolding,” *Nature 2003 426:6968*, vol. 426, no. 6968, pp. 884–890, Dec. 2003, doi: 10.1038/nature02261.

[41] K. A. Dill, S. B. Ozkan, M. S. Shell, and T. R. Weikl, “The Protein Folding Problem,” *Annu Rev Biophys*, vol. 37, pp. 289–316, Jun. 2008, doi: 10.1146/ANNUREV.BIOPHYS.37.092707.153558.

[42] P. G. Wolynes, J. N. Onuchic, and D. Thirumalai, “Navigating the folding routes,” *Science (1979)*, vol. 267, no. 5204, pp. 1619–1620, 1995, doi: 10.1126/science.7886447.

[43] L. Martínez, “Introducing the Levinthal’s protein folding paradox and its solution,” *J Chem Educ*, vol. 91, no. 11, pp. 1918–1923, Nov. 2014, doi: 10.1021/ed300302h.
[44] P. E. Wright and H. J. Dyson, “Intrinsically unstructured proteins: re-assessing the protein structure-function paradigm,” *J Mol Biol*, vol. 293, no. 2, pp. 321–331, Oct. 1999, doi: 10.1006/JMBI.1999.3110.
[45] V. N. Uversky, “Intrinsically disordered proteins and their (disordered) proteomes in neurodegenerative disorders,” *Front Aging Neurosci*, vol. 7, no. 18, 2015, doi: 10.3389/FNAGI.2015.00018.
[46] S. S. Plotkin and J. N. Onuchic, “Understanding protein folding with energy landscape theory. Part I: Basic concepts,” *Q Rev Biophys*, vol. 35, no. 2, pp. 111–167, 2002, doi: 10.1017/S0033583502003761.
[47] R. A. Goldbeck, Y. G. Thomas, E. Chen, R. M. Esquerra, and D. S. Kliger, “Multiple pathways on a protein-folding energy landscape: Kinetic evidence,” *Proc Natl Acad Sci U S A*, vol. 96, no. 6, pp. 2782–2787, Mar. 1999, doi: 10.1073/PNAS.96.6.2782/ASSET/434BD5E4-883A-47D7-A1A0-1EDD96971D8D/ASSETS/GRAPHIC/PQ0592678004.JPEG.
[48] H. Yu *et al.*, “Direct observation of multiple misfolding pathways in a single prion protein molecule,” *Proc Natl Acad Sci U S A*, vol. 109, no. 14, pp. 5283–5288, Apr. 2012, doi: 10.1073/PNAS.1107736109/SUPPL_FILE/PNAS.1107736109_SI.PDF.
[49] H. R. Saibil, “Chaperone machines for protein folding, unfolding and disaggregation,” *Nat Rev Mol Cell Biol*, vol. 14, no. 10, pp. 630–642, Sep. 2013.
[50] F. U. Hartl and M. Hayer-Hartl, “Protein folding. Molecular chaperones in the cytosol: From nascent chain to folded protein,” *Science (1979)*, vol. 295, no. 5561, pp. 1852–1858, Mar. 2002, doi: 10.1126/science.1068408.
[51] A. L. Goldberg, “Protein degradation and protection against misfolded or damaged proteins,” *Nature 2003 426:6968*, vol. 426, no. 6968, pp. 895–899, Dec. 2003, doi: 10.1038/nature02263.
[52] B. Bukau and A. L. Horwich, “The Hsp70 and Hsp60 Chaperone Machines,” *Cell*, vol. 92, no. 3, pp. 351–366, Feb. 1998, doi: 10.1016/S0092-8674(00)80928-9.
[53] G. E. O. Borgstahl and R. E. Oberley-Deegan, “Superoxide Dismutases (SODs) and SOD Mimetics,” *Antioxidants 2018, Vol. 7, Page 156*, vol. 7, no. 11, p. 156, Nov. 2018, doi: 10.3390/ANTIOX7110156.
[54] Y. Furukawa and T. V. O’Halloran, “Posttranslational modifications in Cu,Zn-superoxide dismutase and mutations associated with amyotrophic lateral sclerosis,” *Antioxid Redox Signal*, vol. 8, no. 5–6, pp. 847–867, May 2006, doi: 10.1089/ARS.2006.8.847.
[55] P. J. Hart *et al.*, “A structure-based mechanism for copper-zinc superoxide dismutase,” *Biochemistry*, vol. 38, no. 7, pp. 2167–2178, Feb. 1999, doi: 10.1021/BI982284U.
[56] N. A. Alemasov, N. V. Ivanisenko, S. Ramachandran, and V. A. Ivanisenko, “Molecular mechanisms underlying the impact of mutations in SOD1 on its conformational properties associated with amyotrophic lateral sclerosis as revealed with molecular modelling,” *BMC Struct Biol*, vol. 18, no. 1, pp. 1–14, Feb. 2018, doi: 10.1186/S12900-018-0080-9/TABLES/3.

[57] J. A. Tainer, E. D. Getzoff, J. S. Richardson, and D. C. Richardson, “Structure and mechanism of copper, zinc superoxide dismutase,” *Nature 1983 306:5940*, vol. 306, no. 5940, pp. 284–287, 1983, doi: 10.1038/306284a0.

[58] S. Antonyuk *et al.*, “Structural consequences of the familial amyotrophic lateral sclerosis SOD1 mutant His46Arg,” *Protein Sci*, vol. 14, no. 5, p. 1213, May 2005, doi: 10.1110/PS.041256705.

[59] E. D. Getzoff *et al.*, “Faster superoxide dismutase mutants designed by enhancing electrostatic guidance,” *Nature*, vol. 358, no. 6384, pp. 347–351, 1992, doi: 10.1038/358347a0.

[60] I. Sirangelo and C. Iannuzzi, “The Role of Metal Binding in the Amyotrophic Lateral Sclerosis-Related Aggregation of Copper-Zinc Superoxide Dismutase,” *Molecules 2017, Vol. 22, Page 1429*, vol. 22, no. 9, p. 1429, Aug. 2017, doi: 10.3390/MOLECULES22091429.

[61] J. S. Valentine, P. A. Doucette, and S. Z. Potter, “Copper-zinc superoxide dismutase and amyotrophic lateral sclerosis,” *Annu Rev Biochem*, vol. 74, pp. 563–593, 2005, doi: 10.1146/ANNUREV.BIOCHEM.72.121801.161647.

[62] J. M. Leitch, P. J. Yick, and V. C. Culotta, “The Right to Choose: Multiple Pathways for Activating Copper,Zinc Superoxide Dismutase,” *J Biol Chem*, vol. 284, no. 37, p. 24683, Sep. 2009, doi: 10.1074/JBC.R109.040410.

[63] Y. Furukawa and T. V. O’Halloran, “Amyotrophic lateral sclerosis mutations have the greatest destabilizing effect on the apo- and reduced form of SOD1, leading to unfolding and oxidative aggregation,” *Journal of Biological Chemistry*, vol. 280, no. 17, pp. 17266–17274, Apr. 2005, doi: 10.1074/jbc.M500482200.

[64] R. Fukuhara, T. Tezuka, and T. Kageyama, “Structure, molecular evolution, and gene expression of primate superoxide dismutases,” *Gene*, vol. 296, no. 1–2, pp. 99–109, Aug. 2002, doi: 10.1016/S0378-1119(02)00837-5.

[65] O. Pansarasa, M. Bordoni, L. Diamanti, D. Sproviero, S. Gagliardi, and C. Cereda, “Sod1 in amyotrophic lateral sclerosis: ‘ambivalent’ behavior connected to the disease,” *Int J Mol Sci*, vol. 19, no. 5, May 2018, doi: 10.3390/ijms19051345.

[66] T. Fujisawa *et al.*, “A novel monoclonal antibody reveals a conformational alteration shared by amyotrophic lateral sclerosis-linked SOD1 mutants,” *Ann Neurol*, vol. 72, no. 5, pp. 739–749, Nov. 2012, doi: 10.1002/ANA.23668.

[67] T. Ratovitski *et al.*, “Variation in the Biochemical/Biophysical Properties of Mutant Superoxide Dismutase 1 Enzymes and the Rate of Disease Progression in Familial Amyotrophic Lateral Sclerosis Kindreds,” *Hum Mol Genet*, vol. 8, no. 8, pp. 1451–1460, Aug. 1999, doi: 10.1093/HMG/8.8.1451.

[68] P. M. Andersen *et al.*, “Phenotypic heterogeneity in motor neuron disease patients with CuZn-superoxide dismutase mutations in Scandinavia.,” *Brain*, vol. 120, no. 10, pp. 1723–1737, Oct. 1997, doi: 10.1093/BRAIN/120.10.1723.

[69] L. J. Hayward *et al.*, “Decreased metallation and activity in subsets of mutant superoxide dismutases associated with familial amyotrophic lateral sclerosis,” *Journal of Biological Chemistry*, vol. 277, no. 18, pp. 15923–15931, May 2002, doi: 10.1074/jbc.M112087200.

[70] R. L. Redler, K. C. Wilcox, E. A. Proctor, L. Fee, M. Caplow, and N. V. Dokholyan, “Glutathionylation at Cys-111 induces dissociation of wild type and FALS mutant SOD1 dimers,” *Biochemistry*, vol. 50, no. 32, pp. 7057–7066, Aug. 2011, doi: 10.1021/BI200614Y/SUPPL_FILE/BI200614Y_SI_001.PDF.

[71] A. Tiwari and L. J. Hayward, “Familial amyotrophic lateral sclerosis mutants of copper/zinc superoxide dismutase are susceptible to disulfide reduction,” *Journal of Biological Chemistry*, vol. 278, no. 8, pp. 5984–5992, Feb. 2003, doi: 10.1074/jbc.M210419200.

[72] D. R. Rosen *et al.*, “A frequent ala 4 to val superoxide dismutase-1 mutation is associated with a rapidly progressive familial amyotrophic lateral sclerosis,” *Hum Mol Genet*, vol. 3, no. 6, pp. 981–987, Jun. 1994, doi: 10.1093/HMG/3.6.981.

[73] W. Robberecht *et al.*, “Cu/Zn superoxide dismutase activity in familial and sporadic amyotrophic lateral sclerosis,” *J Neurochem*, vol. 62, no. 1, pp. 384–387, 1994, doi: 10.1046/J.1471-4159.1994.62010384.X.

[74] D. R. Borchelt *et al.*, “Superoxide dismutase 1 with mutations linked to familial amyotrophic lateral sclerosis possesses significant activity.,” *Proc Natl Acad Sci U S A*, vol. 91, no. 17, p. 8296, Aug. 1994, doi: 10.1073/PNAS.91.17.8292.

[75] L. R. Fischer *et al.*, “SOD1 targeted to the mitochondrial intermembrane space prevents motor neuropathy in the Sod1 knockout mouse,” *Brain*, vol. 134, no. 1, pp. 196–209, Jan. 2011, doi: 10.1093/BRAIN/AWQ314.

[76] L. I. Bruijn *et al.*, “Aggregation and Motor Neuron Toxicity of an ALS-Linked SOD1 Mutant Independent from Wild-Type SOD1,” *Science (1979)*, vol. 281, no. 5384, pp. 1851–1854, Sep. 1998, doi: 10.1126/SCIENCE.281.5384.1851.

[77] M. Wiedau-Pazos *et al.*, “Altered Reactivity of Superoxide Dismutase in Familial Amyotrophic Lateral Sclerosis,” *Science (1979)*, vol. 271, no. 5248, pp. 515–518, Jan. 1996, doi: 10.1126/SCIENCE.271.5248.515.

[78] J. S. Beckman, M. Carson, C. D. Smith, and W. H. Koppenol, “ALS, SOD and peroxynitrite,” *Nature 1993 364:6438*, vol. 364, no. 6438, pp. 584–584, 1993, doi: 10.1038/364584a0.

[79] A. C. Estévez *et al.*, “Induction of Nitric Oxide -- Dependent Apoptosis in Motor Neurons by Zinc-Deficient Superoxide Dismutase,” *Science (1979)*, vol. 286, no. 5449, pp. 2498–2500, Dec. 1999, doi: 10.1126/SCIENCE.286.5449.2498.

[80] P. Pasinelli and R. H. Brown, “Molecular biology of amyotrophic lateral sclerosis: insights from genetics,” *Nat Rev Neurosci*, vol. 7, no. 9, pp. 710–723, Sep. 2006, doi: 10.1038/nrn1971.

[81] P. K. Andrus, T. J. Fleck, M. E. Gurney, and E. D. Hall, “Protein Oxidative Damage in a Transgenic Mouse Model of Familial Amyotrophic Lateral Sclerosis,” *J Neurochem*, vol. 71, no. 5, pp. 2041–2048, 1998, doi: 10.1046/J.1471-4159.1998.71052041.X.

[82] I. Ramirez, “Thresholds for starch and Polycose® are lower than for sucrose in rats,” *Physiol Behav*, vol. 50, no. 4, pp. 699–703, 1991, doi: 10.1016/0031-9384(91)90005-9.

[83] P. C. Wong *et al.*, “Copper chaperone for superoxide dismutase is essential to activate mammalian Cu/Zn superoxide dismutase,” *Proc Natl Acad Sci U S A*, vol. 97, no. 6, p. 2891, Mar. 2000, doi: 10.1073/PNAS.040461197.

[84] J. Wang *et al.*, “Copper-binding-site-null SOD1 causes ALS in transgenic mice: aggregates of non-native SOD1 delineate a common feature,” *Hum Mol Genet*, vol. 12, no. 21, pp. 2753–2764, Nov. 2003, doi: 10.1093/HMG/DDG312.

[85] P. A. Jonsson *et al.*, “Minute quantities of misfolded mutant superoxide dismutase-1 cause amyotrophic lateral sclerosis,” *Brain*, vol. 127, no. 1, pp. 73–88, Jan. 2004, doi: 10.1093/BRAIN/AWH005.

[86] N. Shibata, K. Asayama, A. Hiratno, and M. Kobayashi, “Immunohistochemical Study on Superoxide Dismutases in Spinal Cords from Autopsied Patients with Amyotrophic Lateral Sclerosis,” *Dev Neurosci*, vol. 18, no. 5–6, pp. 492–498, Dec. 1996, doi: 10.1159/000111445.

[87] C. Cheroni, M. Peviani, P. Cascio, S. DeBiasi, C. Monti, and C. Bendotti, “Accumulation of human SOD1 and ubiquitinated deposits in the spinal cord of SOD1G93A mice during motor neuron disease progression correlates with a decrease of proteasome,” *Neurobiol Dis*, vol. 18, no. 3, pp. 509–522, Apr. 2005, doi: 10.1016/J.NBD.2004.12.007.

[88] X. Zhang, “Role of Misfolded SOD1 in Neurodegenerative Diseases,” PhD Thesis, University of Manitoba, Winnipeg, Manitoba, 2019.

[89] G. C. Telling *et al.*, “Evidence for the Conformation of the Pathologic Isoform of the Prion Protein Enciphering and Propagating Prion Diversity,” *Science (1979)*, vol. 274, no. 5295, pp. 2079–2082, Dec. 1996, doi: 10.1126/SCIENCE.274.5295.2079.

[90] R. Chia, M. H. Tattum, S. Jones, J. Collinge, E. M. C. Fisher, and G. S. Jackson, “Superoxide Dismutase 1 and tgSOD1G93A Mouse Spinal Cord Seed Fibrils, Suggesting a Propagative Cell Death Mechanism in Amyotrophic Lateral Sclerosis,” *PLoS One*, vol. 5, no. 5, p. e10627, 2010, doi: 10.1371/JOURNAL.PONE.0010627.

[91] L. I. Grad *et al.*, “Intermolecular transmission of superoxide dismutase 1 misfolding in living cells,” *Proc Natl Acad Sci U S A*, vol. 108, no. 39, pp. 16398–16403, Sep. 2011, doi: 10.1073/PNAS.1102645108/SUPPL_FILE/PNAS.201102645SI.PDF.

[92] C. Münch, J. O’Brien, and A. Bertolotti, “Prion-like propagation of mutant superoxide dismutase-1 misfolding in neuronal cells,” *Proc Natl Acad Sci U S A*, vol. 108, no. 9, pp. 3548–3553, Mar. 2011, doi: 10.1073/PNAS.1017275108/SUPPL_FILE/PNAS.1017275108_SI.PDF.

[93] A. L. Horwich and J. S. Weissman, “Deadly Conformations—Protein Misfolding in Prion Disease,” *Cell*, vol. 89, no. 4, pp. 499–510, May 1997, doi: 10.1016/S0092-8674(00)80232-9.

[94] H. Witan *et al.*, “Wild-type Cu/Zn superoxide dismutase (SOD1) does not facilitate, but impedes the formation of protein aggregates of amyotrophic lateral sclerosis causing mutant SOD1,” *Neurobiol Dis*, vol. 36, no. 2, pp. 331–342, Nov. 2009, doi: 10.1016/J.NBD.2009.07.024.

[95] M. Prudencio, A. Durazo, J. P. Whitelegge, and D. R. Borchelt, “An examination of wild-type SOD1 in modulating the toxicity and aggregation of ALS-associated

mutant SOD1," *Hum Mol Genet*, vol. 19, no. 24, p. 4789, Dec. 2010, doi: 10.1093/HMG/DDQ408.

[96] L. I. Grad and N. R. Cashman, "Prion-like activity of Cu/Zn superoxide dismutase: implications for amyotrophic lateral sclerosis," *Prion*, vol. 8, no. 1, pp. 33–41, 2014, doi: 10.4161/PRI.27602.

[97] M. Prudencio, P. J. Hart, D. R. Borchelt, and P. M. Andersen, "Variation in aggregation propensities among ALS-associated variants of SOD1: Correlation to human disease," *Hum Mol Genet*, vol. 18, no. 17, pp. 3217–3226, Sep. 2009, doi: 10.1093/HMG/DDP260.

[98] C. Münch and A. Bertolotti, "Exposure of Hydrophobic Surfaces Initiates Aggregation of Diverse ALS-Causing Superoxide Dismutase-1 Mutants," *J Mol Biol*, vol. 399, no. 3–3, p. 525, Jun. 2010, doi: 10.1016/J.JMB.2010.04.019.

[99] Q. Wang, J. L. Johnson, N. Y. R. Agar, and J. N. Agar, "Protein Aggregation and Protein Instability Govern Familial Amyotrophic Lateral Sclerosis Patient Survival," *PLoS Biol*, vol. 6, no. 7, p. e170, Jul. 2008, doi: 10.1371/JOURNAL.PBIO.0060170.

[100] K. P. Neupane, A. Narayan, S. Sen Mojumdar, G. Adhikari, C. Garen, and M. T. Woodside, "Direct observation of prion-like propagation of misfolding in single protein molecules," *Biophys J*, vol. 121, no. 3, p. 417a, Feb. 2022, doi: 10.1016/J.BPJ.2021.11.675.

[101] S. Sen Mojumdar *et al.*, "Partially native intermediates mediate misfolding of SOD1 in single-molecule folding trajectories," *Nature Communications 2017 8:1*, vol. 8, no. 1, pp. 1–11, Dec. 2017, doi: 10.1038/s41467-017-01996-1.

[102] K. Sugaya and I. Nakano, "Prognostic role of 'prion-like propagation' in SOD1-linked familial ALS: an alternative view," *Front Cell Neurosci*, vol. 8, pp. 1–10, Oct. 2014, doi: 10.3389/FNCEL.2014.00359.

[103] M. Van Rosmalen, M. Krom, and M. Merkx, "Tuning the Flexibility of Glycine-Serine Linkers to Allow Rational Design of Multidomain Proteins," *Biochemistry*, vol. 56, no. 50, pp. 6565–6574, Dec. 2017, doi: 10.1021/ACS.BIOCHEM.7B00902/ASSET/IMAGES/LARGE/BI-2017-00902M_0005.JPEG.

[104] T. H. Evers, E. M. W. M. Van Dongen, A. C. Faesen, E. W. Meijer, and M. Merkx, "Quantitative understanding of the energy transfer between fluorescent proteins connected via flexible peptide linkers," *Biochemistry*, vol. 45, no. 44, pp. 13183–13192, Nov. 2006, doi: 10.1021/BI061288T/SUPPL_FILE/BI061288TSI20060627_051611.PDF.

[105] J. Held and S. Van Smaalen, "The active site of hen egg-white lysozyme: flexibility and chemical bonding," *Acta Crystallogr D Biol Crystallogr*, vol. 70, no. Pt 4, p. 1146, Apr. 2014, doi: 10.1107/S1399004714001928.

[106] M. Oliveri, A. Daga, C. Lunardi, R. Navone, R. Millo, and A. Puccetti, "DNase I behaves as a transcription factor which modulates Fas expression in human cells," *Eur J Immunol*, vol. 34, no. 1, pp. 273–279, Jan. 2004, doi: 10.1002/EJI.200223817.

[107] D. Leung, G. Abbenante, and D. P. Fairlie, “Protease inhibitors: current status and future prospects,” *J Med Chem*, vol. 43, no. 3, pp. 305–341, Feb. 2000, doi: 10.1021/JM990412M.
[108] J. E. Noble and M. J. A. Bailey, “Chapter 8 Quantitation of Protein,” *Methods Enzymol*, vol. 463, no. C, pp. 73–95, Jan. 2009, doi: 10.1016/S0076-6879(09)63008-1.
[109] “Absorbance Technology,” Agilent. Accessed: Jan. 06, 2024. [Online]. Available: https://www.agilent.com/en/technology/absorbance%60%60%E3%80%90oaicite:0%E3%80%91%60%60&%238203
[110] J. A. Cooper, B. R. Mintz, S. L. Palumbo, and W. J. Li, “4 - Assays for determining cell differentiation in biomaterials,” *Characterization of Biomaterials*, pp. 101–137, Jan. 2013, doi: 10.1533/9780857093684.101.
[111] P. Arosio, T. P. J. Knowles, and S. Linse, “On the lag phase in amyloid fibril formation,” *Physical Chemistry Chemical Physics*, vol. 17, no. 12, pp. 7606–7618, Mar. 2015, doi: 10.1039/C4CP05563B.
[112] T. C. T. Michaels, D. Qian, A. Šarić, M. Vendruscolo, S. Linse, and T. P. J. Knowles, “Amyloid formation as a protein phase transition,” *Nature Reviews Physics*, vol. 5, no. 7, pp. 379–397, Jul. 2023, doi: 10.1038/S42254-023-00598-9.
[113] D. L. Floyd, S. C. Harrison, and A. M. Van Oijen, “Analysis of Kinetic Intermediates in Single-Particle Dwell-Time Distributions,” *Biophys J*, vol. 99, no. 2, p. 366, Jul. 2010, doi: 10.1016/J.BPJ.2010.04.049.
[114] H. X. Deng *et al.*, “Amyotrophic Lateral Ssclerosis and Structural Defects in Cu,Zn Superoxide Dismutase,” *Science (1979)*, vol. 261, no. 5124, pp. 1047–1051, 1993, doi: 10.1126/SCIENCE.8351519.
[115] I. Rainero *et al.*, “SOD1 missense mutation in an italian family with ALS,” *Neurology*, vol. 44, no. 2, pp. 347–349, 1994, doi: 10.1212/WNL.44.2.347.
[116] T. Segovia-Silvestre, A. L. Andreu, C. Vives-Bauza, E. Garcia-Arumi, C. Cervera, and J. Gamez, “A novel exon 3 mutation (D76V) in the SOD1 gene associated with slowly progressive ALS,” *Amyotrophic Lateral Sclerosis and Other Motor Neuron Disorders*, vol. 3, no. 2, pp. 69–74, 2002, doi: 10.1080/146608202760196039.
[117] X. Cao *et al.*, “Structures of the G85R Variant of SOD1 in Familial Amyotrophic Lateral Sclerosis,” *J Biol Chem*, vol. 283, no. 23, p. 16177, Jun. 2008, doi: 10.1074/JBC.M801522200.
[118] L. Banci *et al.*, “SOD1 and Amyotrophic Lateral Sclerosis: Mutations and Oligomerization,” *PLoS One*, vol. 3, no. 2, p. e1677, Feb. 2008, doi: 10.1371/JOURNAL.PONE.0001677.
[119] M. Ikeda *et al.*, “Variable clinical symptoms in familial amyotrophic lateral sclerosis with a novel point mutation in the Cu/Zn superoxide dismutase gene,” *Neurology*, vol. 45, no. 11, pp. 2038–2042, 1995, doi: 10.1212/WNL.45.11.2038.